INVESTIGATING THE SHRINKAGE BEHAVIOUR OF REINFORCED CONCRETE SLABS-ON-GROUND

MSc THESIS

WONDMIENEH LAKEW GELAW

HAWASSA UNIVERSITY INSTITUTE OF TECHNOLOGY, HAWASSA, ETHIOPIA

MARCH, 2021

INVESTIGATING THE SHRINKAGE BEHAVIOUR OF REINFORCED CONCRETE SLABS-ON-GROUND

WONDMIENEH LAKEW GELAW

A THESIS SUBMITTED TO THE

DEPARTMENT OF CIVIL ENGINEERING, FACULTY OF CIVIL AND BUILT ENVIRONMENT,

HAWASSA UNIVERSITY INSTITUTE OF TECHNOLOGY, SCHOOL OF

GRADUATE STUDIES

HAWASSA UNIVERSITY

HAWASSA, ETHIOPIA

IN PARTIAL FULFILLMENT OF THE

REQUIREMENTS FOR THE

DEGREE OF

MASTER OF SCIENCE IN STRUCTURAL ENGINEERING

MARCH, 2021

SCHOOL OF GRADUATE STUDIES

HAWASSA UNIVERSITY

ADVISOR'S APPROVAL SHEET

This is to certify that the thesis entitled 'Investigating the Shrinkage Behaviour of Reinforced Concrete Slabs-on-Ground' submitted in partial fulfillment of the requirements for the degree of master's with specialization in structural engineering, the graduate program of the department of civil engineering, faculty of civil and built environment, and has been carried out by Wondmieneh Lakew Gelaw Id No. GPStru R/021/11, under our supervision. Therefore we recommend that the student has fulfilled the requirements and hence hereby can submit the thesis to the department.

Temesgen Wondimu (PhD.)	______________	______________
Name of Major Advisor	Signature	Date
Surafel Tsegaye	______________	______________
Name of Co-advisor	Signature	Date

SCHOOL OF GRADUATE STUDIES

HAWASSA UNIVERSITY

EXAMINER'S APPROVAL SHEET

We, the underside, members of the Board of Examiners of the final open defense by Wondmieneh Lakew have read and evaluated his thesis entitled 'Investigating the Shrinkage Behaviour of Reinforced Concrete Slabs-on-Ground', and examined the candidate. This is, therefore, to certify that the thesis has been accepted in partial fulfillment of the requirements for the degree.

Dr. Temesgen Wondimu	________________	______________
Name of Major Advisor	Signature	Date
Asnake Kefelegn	________________	______________
Name of Internal Examiner-I	Signature	Date
Samuel Tilahun	________________	______________
Name of Internal Examiner-II	Signature	Date
Dr. Binaya Patnaik	________________	______________
Name of External Examiner	Signature	Date
____________________	________________	______________
SGS Approval	Signature	Date

DECLARATION

I hereby declare that this thesis work entitled 'Investigating the Shrinkage Behaviour of Reinforced Concrete Slabs-on-Ground' is my original work and has not been presented for a degree in any other university, and all sources of materials used for this thesis have been duly acknowledged.

Name: Wondmieneh Lakew

Signature: ______________

ACKNOWLEDGEMENT

I gratefully acknowledge my advisor Dr. Temesgen Wondimu for his continuous assistance throughout the entire work. His advice on technical as well as non-technical matters is greatly appreciated. And also I would like to thank my co-advisor Mr. Surafel Tsegaye for his guidance and expert advice. Moreover, I would like to acknowledge the financial support of ERA.

DEDICATION

I would like to thank almighty God for his blessings and helping throughout my research work. And also to pass various obstacles and come up with the accomplishment of this study.

Foremost I would like to dedicate this dissertation to my parents and friends who financially support me, especially Enchalew Wassie, Sileshi Ejigu, Teshome Tilahun, Getnet Mengistu, Yitayal Wondim, Habitamu Alebachew, Meaza Sirgew, Mastewal Eshetu, and Tesfaye Tilahun.

ACRONYMS AND ABBREVIATIONS

AASHTO	American Association of State Highway and Transportation Officials
ACI	American Concrete Institute
ASTM	American Society for Testing and Materials
CAE	Complete Abaqus Environment
CDPM	Concrete Damage Plasticity Model
EC	European Code
E_{cm28}	Mean elastic modulus of concrete at 28 days, MPa
ERA	Ethiopian Road Authority
f_{ck}	Characteristic cylinder strength
f_{cm}	Mean compressive cylinder strength of concrete, MPa
f_{cm28}	Mean compressive cylinder strength of concrete at 28 days, MPa
FEA	Finite Element Analysis
f_y	Yield strength of steel
h	Relative humidity expressed as a decimal
h_o	Notional size of concrete
NORAD	Norwegian Agency for Development Cooperation
RC	Reinforced Concrete
t	Age of Concrete, days
$t - t_c$	Duration of drying, days
V/S	Volume-surface ratio, mm
α	Coefficient of thermal expansion of concrete
ε_{shu}	Notional ultimate shrinkage strain, mm/mm
μ	Coefficient of friction or micro (10^{-6})

TABLE OF CONTENTS

LIST OF TABLES

LIST OF FIGURES

ABSTRACT

Slabs-on-ground are large planes lying on continuous support subjected to defferential shrinkage and loads. Curling or vertical deflection and cracking due to damages of slabs are undesired events caused by differential shrinkage, which limits the service life of the slabs. Typically the slabs-on-ground are exposed to varying relative humidity on the top surface but not at the bottom ground surface, which results in the formation of moisture gradients through the slab, thereby inducing gradient shrinkage, promoting damage and deflection. Referring to service conditions, it is well known that the concrete shrinkage effect tends to be the principal reason for the initial tensile damage to form crack on the top surface and edge curling of slabs-on-ground. Shrinkage strain distribution across the depth of the slab-on-ground was modeled and applied as equivalent temperature gradient. This thesis intends to investigate the shrinkage behavior of reinforced concrete slabs-on-ground for different parametric studies using the non-linear finite element analysis software package, Abaqus. The general purpose finite element software Abaqus used to simulate analysis of slab-on-groud in this study has no defined program for shrinkage analysis so that equivalent temperature gradient was used to simulate shrinkage distribution. The models are verified by comparing the results with previous experimental studies. Based on the performed parametric studies, upward curling was maximum at corner of free end slabs and steel reinforcement positioned in center of the slab can minimize tensile damage to reduce top surface cracking of slabs-on-ground.

Keywords: Abaqus, curling, damage, finite element, gradient shrinkage, slabs-on-ground.

CHAPTER ONE

INTRODUCTION

1.1 Background of the Study

According to ACI 360R-06, slab-on-ground is defined as a slab, supported by the ground, whose main purpose is to support the applied loads by bearing on the ground (ACI 360R-10, 2010). From a structural point, slabs on the ground are large planes lying on continuous support (Øverli, 2014). Reinforced concrete slabs-on-ground are commonly used in many industrial floors, warehouses, airport and highway pavements, parking lot slabs, and buildings (Prakash, 2018).

Serviceability requirements of structures refer to the behavior of structures at working loads and they are satisfied when the structure does not deflect or crack more than certain limits provided by the building codes (ES EN, 1992:2015). Both cracking and deflection are primarily dependent on the properties and behavior of the concrete but are more difficult to predict because of the non-linear, inelastic, and time-dependent (e.g shrinkage) nature of the concrete. If structural designers do not adequately account for this non-linear behavior, serviceability problems may result (Nejadi, 2005).

The primary cause of shrinkage is the loss of water from the concrete during drying. The shrinkage process starts at the surface of a concrete specimen and gradually penetrates the center. This results in a non-uniform distribution of shrinkage known as differential shrinkage. In concrete design and analysis, shrinkage is usually considered to be uniform. (Rebello, 1990). The most important factors that influence shrinkage of concrete relative humidity, the dimension of the element, and the composition of the concrete (ES EN, 1992:2015).

Drying shrinkage is often a major problem in concrete slabs-on-ground, causing cracks on the top surface before any live loads are applied. Shrinkage can lead to significant tensile stresses in slabs on the ground due to the one-side drying on the top surface. This can especially be a problem in areas with hogging moments, but even without any applied external load, top-side cracking could occur (Øverli, 2014).

For shrinkage strains to cause stresses in a structure, there must be some kind of restraints from the geometrical shape or supports (Øverli, 2014). For slabs-on-ground, several other restraints also prevent the concrete from shrinking freely. These include for example friction to the sub-base and local slab thickenings. As the restraints prevent free movements and induce tensile stresses, cracking can occur if the stresses reach the tensile strength of the concrete. Cracks in floors are undesired since they precipitate degradation as well as being aesthetically unappealing (Fabian Narin and Olle Wiklund, 2012).

In many situations, cracking in reinforced concrete structures is inevitable. Cracks occur wherever and whenever the tensile stress in the concrete reaches the tensile strength of the concrete. After the concrete sets and hardens, tensile stress at any location may be caused by many different factors, including early-age heat of hydration, applied loads, restrained shrinkage, temperature changes, settlement of supports, and so on. Cracks caused by restraint to load-independent deformation, including deformations due to early-age cooling, shrinkage, or ambient temperature changes, are termed intrinsic cracks. After cracking, further shrinkage-induced deformation causes significant increases in crack widths with time (Gilbert, 2017).

Many variables influence the width and spacing of intrinsic cracks, including the quantity, orientation, and distribution of the reinforcement crossing the crack, the cover to the reinforcement, the bond characteristics of the reinforcement, the deformational properties of the concrete (including its creep and shrinkage characteristics), the environment and the size of the member. Considerable variations exist in the crack width from crack to crack and in the spacing between adjacent cracks, because of random variations in the properties of the in-situ concrete (Gilbert, 2017).

Due to the large likelihood and economic consequences related to shrinkage cracks, the economic risk is high. Studies regarding how the number of damages caused by shrinkage cracking can be reduced are consequently of high relevance and there is a need for a better design approach when designing concrete floors concerning shrinkage cracking. (Fabian Narin and Olle Wiklund, 2012).

Shrinkage of concrete depends on several known phenomena acting during different time-spans of the concrete life cycle. The general factor affecting the shrinkage is volume reduction due to loss of water. Shrinkage leads to cracking if it is restrained and if the stresses from the restrained situation reach values equal to the tensile capacity of the concrete in any section. Chemical reactions in the concrete cause water movement inside the structure and as the hydration processes continue over time, this is a complex situation. Chemical and autogenous shrinkage is fundamentally based and defined by these chemical reactions. They are both internal phenomena, occurring without moisture exchange with the external environment. (Fabian Narin and Olle Wiklund, 2012).

The prime asset of many buildings is the concrete ground floor. If the floor becomes unusable, for reasons of structural integrity or surface irregularity, the operation of the building can be seriously disrupted and the capital value of the entire structure put at risk. At present, there is a lack of understanding of concrete floor slab construction materials and their behavior, reacted in current design practice, and improvements are needed if effective and economic engineering solutions to the increasing demands being placed on floors by the end-users are to be achieved. (P. J. Robins *et al*., 2003).

Due to the relatively low tensile strength of concrete, cracks are inevitable in reinforced concrete structures. Therefore, studying the cracking behavior of reinforced concrete elements and controlling the width of cracks are necessary objectives both in research and in design. (Nejadi, 2005).

1.2 Statement of the Problem

The primary cause of shrinkage is the loss of water from the concrete during drying. The shrinkage process starts at the surface of a concrete specimen and gradually penetrates the center. Typically the slabs-on-ground are exposed to varying relative humidity on the top surface but not at the bottom ground surface, which results from the formation of moisture gradients through the slab, which inducing nonlinear gradient shrinkage across the thickness of the slabs. However, in concrete design and analysis, shrinkage is usually considered to be uniform. A common problem with slabs-on-ground is that concrete slabs curling upward (or vertical deflection) due to nonlinear gradient shrinkage, caused by negative moisture gradients. Also tensile damage (or cracking) and principal stress because of drying shrinkage are inevitable problems, which will affect the serviceability of the structure.

1.3 Objectives of the Study

The objective of the thesis is to analyze the shrinkage behavior of reinforced concrete slabs-on-ground by using non-linear FEM.

1.3.1 General objective

The main objective of the thesis is to investigate the shrinkage behavior of reinforced concrete slabs-on-ground using FEM, Abaqus/CAE.

1.3.2 Specific objectives

- To investigate deflection of reinforced concrete slabs-on-ground subjected to differential shrinkage distribution.
- To evaluate maximum principal stress for reinforced concrete slabs-on-ground due to drying shrinkage.
- To study tensile damage that causes cracking of reinforced concrete slabs-on-ground subjected to nonlinear shrinkage distribution.
- To perform the effect of parameters on how to influence deflection, stress, and damage in reinforced concrete slabs-on-ground in the context of drying shrinkage.

1.4 Limitation and Scope of the Study

This study aims to investigate the principal stress, damage, and deflection behavior of RC slabs-on-ground due to shrinkage strain. There are several methods to predict the shrinkage of concrete; in this thesis, only three methods are involved. Also since it is not possible to consider all types of concrete and conditions which will affect the outcome, only normal strength type of concrete C20/25, C25/30, and C30/37 are common in the practice of construction of slabs on the ground, taken as an example in this paper. The slab is focused on slabs-on-ground, where a slab thickness of 80mm, 120mm, and 160mm are chosen, which are the range that is most likely to occur in practice. The effect of temperature, relaxation, and content of steel reinforcement, and creep were not considered in this study.

1.5 Significance of the Study

This study contributes and increases the understanding of the response of reinforced concrete slabs-on-ground subjected to differential shrinkage. The results obtained will be helpful for the construction industry, designers, educational purposes, and next coming researchers in this area. The outcome of the study will add valuable data or information about the behavior of the reinforced concrete slabs-on-ground for one side drying shrinkage. Due to the nonlinear distribution of shrinkage drying across the thickness of the slab, simplified models are not available in educational textbooks and standards including new Ethiopian building codes adopted from Euro Code. Therefore, the goal is to contribute a study on the behavior of reinforced-concrete slabs-on-ground for nonlinear distribution of shrinkage strain as well as provide a tool for further study in the analysis of shrinkage of reinforced concrete slabs-on-ground and the role of finite element software.

1.6 Thesis Structure

This study contains five chapters and appendices at all. The first chapter is an introduction to the thesis which contains the background of the study, statement of the problem, objectives of the study, and the significance of the research. In the second chapter of the thesis, the articles were reviewed which has been conducted before in shrinkage behavior of concrete, slabs-on-ground, and finite element analysis. In the third chapter, materials and methods of simulating in FEA were discussed with their time-dependent property and mechanical property. In the fourth chapter, validations and the results of the parametric studies were discussed consecutively. In the fifth chapter, the conclusion and recommendation were given on the summary of the study are already discussed. For the clearance and resource of materials at the end of the thesis reference and appendix were listed.

CHAPTER TWO

LITERATURE REVIEW

2.1 General

This section provides an overview of previous studies that have been conducted on shrinkage analysis and behavior of slabs-on-ground subjected to time-dependent load. Different articles were reviewed to understand the techniques and key studies that have been conducted.

2.2 Slabs-on-Ground

Slab-on-ground is a slab, supported by the ground, whose main purpose is to support the applied loads by bearing on the ground. The slab support system consists of a subgrade, usually a base, and sometimes a sub base. The properties and dimensions of the slab and the supporting materials are important in the design of a slab-on-ground (ACI 360R-10, 2010). It is better to provide the minimum soil stiffness required to avoid excessive deflections (Amir M. *et al*., 2012). The slab-on-grade is dependent on slab type, support condition, loading type, and function of the building (Shideh Shadravan *et al*., 2015).

2.2.1 Types of slabs-on-ground

Slabs-on-ground may be unreinforced, reinforced, or structural slabs for industrial, commercial, residential, parking lots, and roadway pavements. These slabs have been grouped into four categories based on the amount of reinforcement provided and basic design choices for the construction of slabs-on-ground (ACI 360R-10, 2010), (Gunalan, 1986). These are:

1. Unreinforced concrete slab,

2. Slabs reinforced to limit crack width,

3. Slabs reinforced to prevent cracking, and

4. Structural slabs.

2.2.2 Support systems for slabs-on-ground

From a structural point, slabs on the ground are large planes lying on continuous support. The response of the slab depends on many factors such as loaded area, slab size, subgrade stiffness (Øverli, 2014). The slab support system consists of a subgrade, usually a base, and sometimes a sub-base as illustrated in figure 2.1 below. Crushed rock, gravels, or coarse sands, which have high strength, low compressibility, and high permeability, are commonly used as base courses.

Soils in the subgrade are generally the ultimate supporting materials, but bedrock, competent or weathered, may also be encountered. If the existing soil has uniform strength and other necessary properties to support the slab, the slab may be placed directly on the existing subgrade (ACI 360R-10, 2010).

Because all concrete is permeable to some degree, water and water vapor can move through slabs-on-ground and this can adversely affect the storage of moisture-sensitive products on the slab, humidity control within the building, and a variety of flooring materials from coatings to carpets, vapor retarder/barrier is provided (ACI 360R-10, 2010).

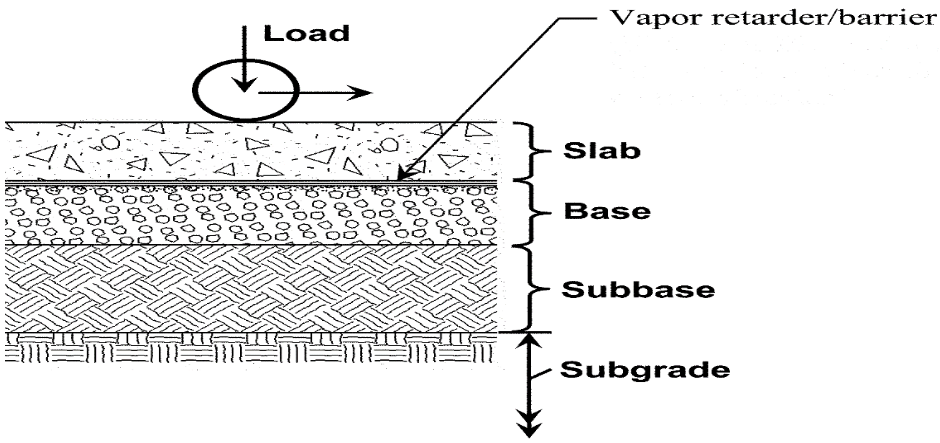

Figure 2.1 Slab support system terminology *(ACI 360R-10, 2010).*

The slab-on-grade performance under static loads strictly depends on the flexural slab stiffness (e.g., slab thickness) and the mechanical properties of the ground. The latter, in practice, are considered by designers using simplified methods. The most commonly used is the Winkler model, which only takes into account the equivalent elastic stiffness exhibited by the ground in presence of vertical displacements perpendicular to the middle slab-plane, Winkler soil stiffness, $K_{Winkler}$ (Giuseppe Tiberti *et al.*, 2018).

Effect of subgrade reaction: Westergaard assumed the slab to be a homogenous, isotropic elastic solid sustained by the reactions from an elastic subgrade which are only vertical and proportional to the deflections of the slab. He introduced the term "modulus of subgrade reaction *k*", which represents the behavior of the subgrade based on the load per unit area causing unit deflection. This behavior is based in principle on the Winkler model, which is traditionally preferred for slab-on-ground design (Amir M. *et al.*,2012).

Different values were assumed for the subgrade reaction parameter (K). The variation of subgrade reaction with slab maximum or mid-span deflection. The mid-span or maximum deflection had a reduced value when the subgrade reaction was increased (Al-Azzawi, 2018).

Friction and restraints: There are two types of restraint conditions depending on the structure's geometry, namely, internal and external restraint. Internal restraint happens when the restraint condition comes from the element itself which is a common problem in thick sections. This is due to out-of-phase deformation of inner and outer parts caused by non-uniform temperature or moisture distribution in the section. The exterior which is exposed to the outside environment cools down or drys faster than the inner section which is shielded. In mass concrete, however, the warmer or moister inner part expands while the outer portion restrains this expansion causing compressive stresses in the inner part and tensile stresses in the outer concrete leading to cracking in the outer surface which is under tension (Matin, 2015).

2.3 Curling of Slabs-on-Ground

The basic cause of curling is differential shrinkage that occurs in a slab as the exposed top surface shrinks and the core does not. Curling of concrete slabs at joints and cracks is directly related to drying shrinkage. Therefore, if an effort is made to reduce drying shrinkage, curling will also be reduced. The terms "curling" and "warping" can be used interchangeably (N. Mailvaganam *et al.*, 2000).

Curling- the distortion of an originally essentially linear or planar member into a curved shape, such as the warping of a slab to differences in temperature or moisture content in the zones adjacent to its opposite faces.

Warping- a deviation of a slab or wall surface from its original shape, usually caused by either temperature or moisture differentials or both within the slab or wall.

Curling occurs at slab edges because of differential shrinkage. The upper part of the slab-on-ground almost always has the greatest shrinkage because the top surface is commonly free to dry faster, and the upper portion has a higher unit water content at the time of the final set. Higher relative humidity in the ambient air at the upper surface will reduce the severity of curling even though the concrete may be a high shrinkage material (ACI 360R-10, 2010).

Upward edge curling already caused by negative moisture gradients can be increased by cold slab surface temperatures or by hotter slab bottom temperatures (Figure 2.2). Vertical deflection is greater at slab corners than at slab edges simply because that is what happens when two adjacent, perpendicular edges in a flat plane both roll upward (Ytterberg, 1992). Such moisture gradients and curling increase when:

- The slab is made from high-shrinkage concrete.
- The slab surface is exposed to low humidity air.
- The subgrade or sub-base under the hardened slab has a high moisture content.
- The concrete has a high modulus of elasticity.

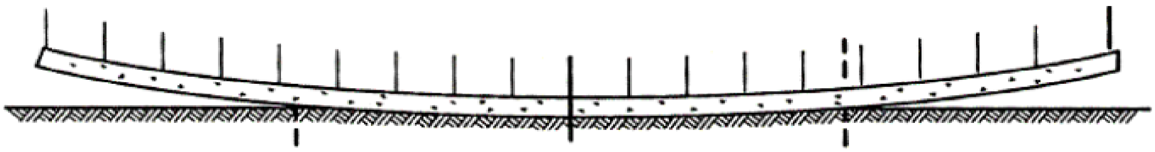

Figure 2. 2 Enclosed slabs curl upward *(Ytterberg, 1992).*

The most common positive temperature gradient with its downward edge curling is that caused by heat from the sun on the upper slab surface (Figure 2.3). Downward curling creates compressive stress at the top surface of the concrete slab, while the bottom is in tension and the reverse is true for upward edge slab curling (Jafarifar, 2012).

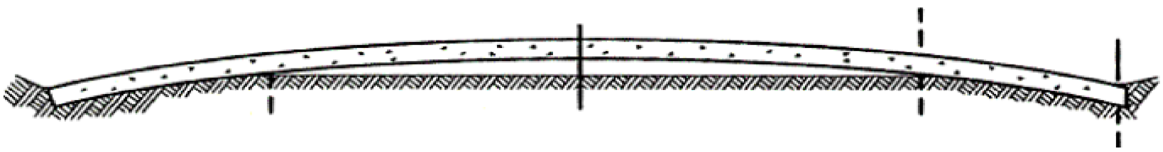

Figure 2. 3 Outdoor slabs exposed to the sun, curl downward *(Ytterberg, 1992).*

2.4 Loads and Shrinkages of Slabs-on-Ground

Slabs-on-ground is subjected to gradient shrinkage strain as well as loads. These loads, shrinkage behavior of concrete slab-on-ground and types of shrinkage are discussed briefly in this section.

2.4.1 Loads of slabs-on-ground

The case studied in (Amir M. *et al*., 2012) paper concerns a load applied at the center of a flat slab resting on the ground. The mode of failure considered is a circular negative failure on the top surface and positive radial failure lines from the load application point to the perimeter of that circle on the bottom surface. It has been proved that as slab plan area increases, settlement decreases due to increased bending action, and the built-up stresses rise as well. Typical loading which influences both serviceability and load capacity are concentrated loads from vehicles, columns, or leg loads from storage platforms (Øverli, 2014).

2.4.2 Shrinkage behavior of concrete slabs-on-ground

Concrete, like many construction materials, is not dimensionally stable when subjected to changes in moisture content. As new slabs dry from the surface down, the moisture gradient through the slab leads to differential shrinkage (N. Mailvaganam *et al*., 2000). The main problems found in industrial floors are related to extensive crack phenomena that often occur before applying the service loads on the pavement. These cracks are generally due to shrinkage effects (and, in some cases, the thermal effects) that mainly develop during the first few weeks after concrete pouring (due to the large size and exposed surface, low thickness, and high degree of restraint). On the contrary, if shrinkage cracks do not early appear, shrinkage stresses will represent an additional contribution to the load effect and may favor cracking phenomena when loads are applied (Giuseppe Tiberti *et al*., 2018).

Because water-primarily leaves the concrete from the upper surface of slabs-on-ground, a moisture gradient is created between the top and bottom of the slab. Such moisture gradients are magnified by moist subgrades and by low humidity at the top surface. Evaporation of moisture from the top surface of a slab causes the upper half of the slab to shrink more than the lower half, although some shrinkage occurs in all three dimensions (ACI 360R-10, 2010).

For slabs-on-ground, the shrinkage restraint from the subgrade varies with the coefficient of friction and planarity of the surface of the sub-base. Thermal movement is caused by a change in slab temperature from that at which the slab was initially placed. It should be taken into account for any floor where the concrete is cast at a significantly different temperature than the normal operating temperature (ACI 360R-10, 2010).

Shrinkage of concrete is a physical property caused by a loss in volume. The main factors affecting this phenomenon are the ambient temperature and humidity, the dimensions of the element, and the composition of the concrete and its curing procedure (Giuseppe Tiberti *et al*., 2018). Usually, the relative humidity will be much higher at the bottom compared to at the top surface and this non-linear drying strain causes the top surface to shrink more than the bottom (Prakash, 2018) as shown in figure 2.4 below.

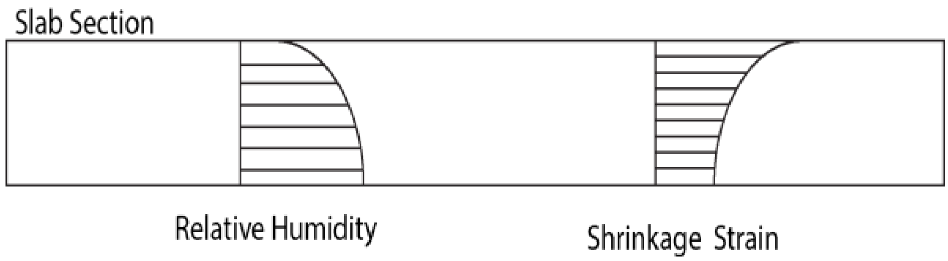

Figure 2. 4 Distribution of relative humidity & shrinkage strain *(Prakash, 2018)*.

Types of shrinkage

For concrete slabs with dense graded sub-bases, the drying occurs from the top surface; thus the (V/S) ratio equals the concrete thickness D. Assumes that the temperature distribution in the concrete slab is constant, with depth as an approximation. Shrinkage of concrete occurs at two different stages (i.e early age and long-term shrinkage) and can be classified into different types (i.e plastic shrinkage, autogenous shrinkage, carbonation shrinkage, and drying shrinkage) (Prakash, 2018).

1. Plastic shrinkage: Plastic shrinkage develops before and during the concrete’s setting process (Freidriks, 2015). As a result of evaporation water is lost from the surface, and due to surface tension and capillary tension forces, the concrete contracts, which is known as plastic shrinkage. Due to plastic shrinkage, the top surface of the concrete becomes harder in comparison with other portions of the concrete and at this stage, the concrete has low tensile strength, which results in the formation of plastic shrinkage cracking (Prakash, 2018).

Plastic shrinkage cracking can effectively be prevented by keeping down the rate of evaporation of water from the surface of concrete: It should be remembered that evaporation is increased when the temperature of the concrete is much higher than the ambient temperature; under such circumstances, plastic shrinkage can occur even if the relative humidity of the air is high. It is, therefore, best to protect the concrete from sun and wind, place and finish fast, and start curing very soon thereafter. Placing concrete on a dry subgrade should be avoided (Freidriks, 2015). Generally, (P J Robins *et al*., 2003) states that plastic shrinkage is not the problem for slabs on the ground.

2. Autogenous shrinkage: The shrinkage occurring in the absence of moisture exchange (as in a sealed concrete specimen) due to the hydration reactions taking place in the cement matrix. Less commonly, it is termed basic shrinkage or chemical shrinkage (ACI 209.2R-08, 2008). Autogenous shrinkage is a consequence of chemical shrinkage, which arises from the reduction in absolute volumes of the solid and liquid phases of the products of hydration compared with absolute volumes of original un-hydrated cement and combined water. Since autogenous shrinkage is caused by self-desiccation, autogenous shrinkage increases with an increase in the amount of finer pore gels and with a decrease in water-cement ratio when the amount of water is decreased to make a low water-cement ratio, the water in pores are quickly consumed by hydration reaction (Freidriks, 2015).

Traditionally, autogenous shrinkage has been neglected from consideration in measurements of total shrinkage. This is because, at normal range water-to-cement ratios, the magnitude of autogenous shrinkage is very small in comparison to drying shrinkage measurements (Freidriks, 2015). Autogenous shrinkage should be considered specifically when new concrete is cast against hardened concrete (ES EN, 1992:2015).

3. Carbonation shrinkage: Carbonation shrinkage occurs due to a chemical reaction between cement constituent, water, and carbon dioxide from the atmosphere during the hardening process of the concrete. The relative humidity of the environment surrounding the concrete plays a vital role in the carbonation process. Comparatively, carbonation shrinkage and autogenous shrinkage are low to plastic and drying shrinkage (Prakash, 2018).

4. Drying shrinkage: Drying shrinkage of concrete is defined as the reduction in concrete volume resulting from a loss of water from the concrete after hardening (Ytterberg, 1992). Drying shrinkage is the response to relative humidity change in the concrete. The volume reduces due to the moisture loss after the concrete has been set. Effectively, this is the drying of the moisture found in the pores on the surface of the exposed concrete. This means that concrete dimensions can play a large role in the degree of drying shrinkage that occurs; the more exposed surface area will lead to a greater amount of shrinkage. In cement-based materials, drying shrinkage of the hardened cement paste matrix leads to stresses and can lead to cracking if the shrinkage is restrained (Freidriks, 2015).

2.5 Cracking due to Drying Shrinkage

Cracks could easily develop as a result of restraining a concrete member since the tensile strain capacity of concrete is usually somewhere in the area of 150×10^{-6} mm/mm or less. Since a wide number of parameters influence the shrinkage in concrete, there is a high degree of uncertainty in the prediction of shrinkage. The composition of concrete, source of aggregate, the geometry of specimen, ambient relative humidity, and the ratio of the exposed surface to the volume of the member are some of the most important factors that influence the concrete shrinkage strain (Matin, 2015).

Internal shrinkage restraint occurs due to moisture gradients before a concrete member reaches moisture equilibrium. This moisture gradient can cause tensile and compressive stresses on the surface and in the interior of the member respectively and this stress causes cracking in the concrete. The concrete member experiencing a contraction due to drying shrinkage could always be subjected to some degree of external restraint. This restraint could be from the sub-base, another part of the structure, or even the reinforcement inside the member. When the shrinkage is restrained, tensile stresses start to develop within the concrete which could cause cracking if they exceed the tensile strength of concrete. Cracks occur as soon as the net tensile stress reaches the tensile strength of concrete. Relative humidity, aggregate type, and content (or paste content), water content, and w/c are the most important parameters that influence the ultimate drying shrinkage. Drying time, distance from the exposed surface, relative humidity, and size of the member are among the parameters that affect the shrinkage and rate of moisture loss in concrete (Matin, 2015).

2.6 Concrete Shrinkage Prediction Models

The models selected for comparison are the Bazant-Baweja B3 model developed by (Zdeněk P. Bažant and Sandeep Baweja, 2000), the CEB-FIP Model Code 90-99 developed by (Telford, 1993), and the GL2000 developed by (Gardner, N. J. and Lockman, M. J., 2000).

Comparison of models with experimental data is complicated by the lack of agreement on the selection of appropriate data and on the methods used to compare the correlation (ACI 209.2R-08, 2008).

1. Bazant-Baweja B3 model

The (Zdeněk P. Bažant and Sandeep Baweja, 2000) B3 model is the latest variant in some shrinkages and creeps prediction methods developed by Bazant and his coworkers at Northwestern University. According to (Zdeněk P. Bažant and Sandeep Baweja, 2000), the B3 model is simpler and is better theoretically justified than the previous models.

The prediction of material parameters of the B3 model is restricted to Portland cement concretes, having 28 days mean cylinder compressive strength varying from 17 to 70 MPa, the water-cement ratio of 0.30 to 0.85, the aggregate-cement ratio of 2.5 to 13.5, and cement content of 160 to 720 kg/m^3. The formulae are valid for concretes cured for at least one day. It is reported that the prediction of concrete outside the limitations stated can be performed using the B3 model if the parameters are calibrated with tests (Zdeněk P. Bažant and Sandeep Baweja, 2000).

The mean shrinkage strain $\varepsilon_{sh}(t, tc)$ in the cross-section at age of concrete *t* (days), measured from the start of drying at t_c (days), is calculated by equation (2.1).

$$\varepsilon_{sh}(t, tc) = -\varepsilon_{sh\infty} K_h S(t - tc) \qquad (2.1).$$

Where $\varepsilon_{sh\infty}$ is the ultimate shrinkage strain, K_h is the humidity dependence factor (Table A.6), $S(t - tc)$ is the time curve, and $(t - tc)$ is the time from the end of the initial curing.

The ultimate shrinkage $\varepsilon_{sh\infty}$ is given by equation (2.2).

$$\varepsilon_{sh\infty} = -\varepsilon_{s\infty} \frac{E_{cm607}}{E_{cm(tc+\tau sh)}} \qquad (2.2).$$

Where $\varepsilon_{s\infty}$ is a constant given in equation (2.3) and $\frac{E_{cm607}}{E_{cm}(tc+\tau sh)}$ is a factor to account for the time dependence of ultimate shrinkage, given in equation (2.4).

$$\varepsilon_{s\infty} = -\alpha_1 \alpha_2 (0.019 w^{2.1} {f_{cm28}}^{-0.28} + 270) x 10^{-6} \qquad (2.3).$$

$$E_{cmt} = E_{cm28} \left\{\frac{t}{4+0.85t}\right\}^{0.5} \qquad (2.4).$$

$$E_{cm28} = 4734\sqrt{f_{cm28}} \quad (2.5).$$

$$f_{cm28} = f'_c + 8.0 \quad (2.6).$$

Where w is the water content in kg/m^3, f_{cm28} is the concrete mean compressive strength at 28 days in MPa, f'_c is the specified/characteristic compressive cylinder strength (MPa) defined as that strength below which 5% of all possible strength measurements for the specified concrete may be expected to fall, and α_1 and α_2 are constants related to the cement type and curing condition. (Note: The negative sign is the model authors' convention.) The values of α_1 and α_2 are given in Tables A.7 and A.8, for cement type and curing conditions respectively. The ambient relative humidity factor K_h given by equation (2.7).

$$K_h = \begin{cases} -0.2\,, & if\ h = 1 \\ 12.74 - 12.94h\,, & if\ 0.98 < h < 1 \\ 1 - h^3\,, & if\ h \le 0.98 \end{cases} \quad (2.7).$$

The time function for shrinkage $S(t - tc)$ is given by equation (2.8).

$$S(t - tc) = tanh\sqrt{\frac{(t-tc)}{\tau_{sh}}} \quad (2.8).$$

Where t and t_c are the age of concrete and the age drying commenced or end of moist curing in days, respectively, and τ_{sh} is the shrinkage half-time in days as given in equation (2.9).

The size dependence of shrinkage is given by

$$\tau_{sh} = 0.085\mathrm{tc}^{-0.08} {f_{cm28}}^{-0.25} \left\{2\mathrm{k_s}\left(\frac{\mathrm{v}}{\mathrm{s}}\right)\right\}^2 \quad (2.9).$$

Where $\mathrm{k_s}$ is the cross-section shape-correction factor (Table A.9), and *V/S* is the volume-surface ratio in mm.

2. CEB - FIP model code 90-99

The (Telford, 1993) model has a similar concept to that of (ACI 209.2R-08, 2008) model in the sense that it gives a hyperbolic change with time for shrinkage, and it also uses an ultimate value corrected according to the mixture to proportioning and environment conditions. Unless special provisions are given, the models for shrinkage predict the time-dependent behavior of ordinary-strength concrete (12 MPa $\le f'_c \le$ 80 MPa) moist cured at normal temperatures not longer than 14 days and exposed to a mean ambient relative humidity in the range of 40 to 100% at mean ambient temperatures from 5 to 30 °C. The models are valid for normal weight plain structural concrete having an average compressive strength in the range of 20 MPa $\leq f_{cm28} \leq$ 90 MPa.

The CEB-FIP Model Code 1990 is produced by the Euro-International Concrete Committee and International Federation for Pre-stressing. The prediction of shrinkage of concrete by the CEB 1990 is restricted to ordinary structural concretes, having 28 days mean cylinder compressive strength varying from 12 to 80 MPa, mean RH 40 to 100% and mean temperature 5 to 30 °C.

The total shrinkage of concrete $\varepsilon_{sh}(t, t_c)$ can be calculated from equation (2.10).

$$\varepsilon_{sh}(t, t_c) = \varepsilon_{cas}(t) + \varepsilon_{cds}(t, t_c) \quad (2.10).$$

Where $\varepsilon_{sh}(t, t_c)$ is the total shrinkage, $\varepsilon_{cas}(t)$ is the autogenous shrinkage, and $\varepsilon_{cds}(t, t_c)$ is the drying shrinkage at concrete age t days after the beginning of drying at tc day.

The autogenous shrinkage component $\varepsilon_{cas}(t)$ is calculated from equation (2.11).

$$\varepsilon_{cas}(t) = \varepsilon_{caso}(f_{cm28})\beta_{as}(t) \quad (2.11).$$

Where $\varepsilon_{caso}(f_{cm28})$ is the notional autogenous shrinkage coefficient and $\beta_{as}(t)$ is the function describing the time development of autogenous shrinkage in equation (2.12) below.

$$\varepsilon_{caso}(f_{cm28}) = -\alpha_{as}\left(\frac{\frac{f_{cm28}}{f_{cmo}}}{6+\frac{f_{cm28}}{f_{cmo}}}\right)^{2.5} x10^{-6} \quad (2.12).$$

$$\beta_{as}(t) = 1 - \exp[-0.2(\frac{t}{t1})^{0.5}] \quad (2.13).$$

Where f_{cm28} is the mean compressive strength of concrete at an age of 28 days (MPa) and $f_{cmo} = 10\ MPa$, t is the concrete age (days), $t_1 = 1\ day$ and α_{as} is a coefficient that depends on the type of cement (Table A.11).

The autogenous shrinkage component is independent of the ambient relative humidity, and the member size and develops more rapidly than drying shrinkage.

The drying shrinkage $\varepsilon_{cds}(t, t_c)$ is calculated from equation (2.14).

$$\varepsilon_{cds}(t, t_c) = \varepsilon_{cdso}(f_{cm28})\beta_{RH}(h)\beta_{ds}(t - tc) \quad (2.14).$$

Where $\varepsilon_{cdso}(f_{cm28})$ is the notional drying shrinkage coefficient from equation (2.15), $\beta_{RH}(h)$ is the coefficient that takes into account the effect of relative humidity on drying shrinkage from equation (2.16), and $\beta_{ds}(t-tc)$ is the function describing the time development of drying shrinkage from equation (2.17).

$$\varepsilon_{cdso}(f_{cm28}) = \{(220 + 110\alpha_{ds1})\exp(-\alpha_{ds2}f_{cm28}/f_{cmo})\}x\, 10^{-6} \quad (2.15).$$

$$\beta_{RH}(h) = \begin{cases} -1.55\left(1-\left(\frac{h}{h_o}\right)^3\right) & \text{for } 0.4 \leq h < 0.99\beta_{s1} \\ 0.25 & \text{for } h \geq 0.99\beta_{s1} \end{cases} \quad (2.16).$$

$$\beta_{ds}(t-tc) = \left[\frac{(t-t_c)/t_1}{350\{(\frac{V}{S})\div(\frac{V}{S})_o\}^2 + (t-t_c)/t_1}\right]^{0.5} \quad (2.17).$$

$$\beta_{s1} = \left(\frac{3.5f_{cmo}}{f_{cm28}}\right)^{0.1} \leq 1.0 \quad (2.18).$$

$$f_{cm28} = f'_c + 8.0 \quad (2.19).$$

Where α_{ds1} and α_{ds2} are coefficients that depend on the type of cement (Table A.11), β_{s1} is a coefficient that takes into account the self-desiccation in high-performance concrete, *h* is the ambient relative humidity as a decimal, h_o= 1, *V/S* is the volume-surface ratio (mm), $(V/S)_0$ = 50 mm, f_{cmo} = 10 MPa, t_c is the concrete age at the beginning of drying (days), $(t - t_c)$ is the duration of drying (days), and f'_c is the specified/characteristic compressive cylinder strength (MPa) defined as that strength below which 5% of all possible strength measurements for the specified concrete may be expected to fall.

According to equation (2.23) for normal-strength concretes, swelling is to be expected if the concrete is exposed to an ambient relative humidity near 99%. For higher-strength grades, swelling will occur at lower relative humidities because of the preceding reduction of the internal relative humidity due to self-desiccation of the concrete.

3. GL2000 model

The model presented herein corresponds to the last version of the GL2000 model, including minor modifications to some coefficients and the strength development with the time equation of the original model developed by (Gardner, N. J. and Lockman, M. J., 2000). It is a modified Atlanta 97 model (ACI 209.2R-08, 2008), which itself was influenced by CEB MC90. It presents a design-office procedure for calculating the shrinkage of normal-strength concretes, defined as concretes with mean compressive strengths less than 82 MPa that do not experience self-desiccation, using the information available at design, namely, the 28-day specified concrete strength, the concrete strength at loading, element size, and relative humidity. According to (Gardner, N. J. and Lockman, M. J., 2000), the method can be used regardless of what chemical admixtures or mineral by-products are in the concrete, casting temperature, or curing regime. The predicted values can be improved by simply measuring concrete strength development with time and modulus of elasticity.

Shrinkage strain $\varepsilon_{sh}(t, t_c)$ is calculated from equation (2.20).

$$\varepsilon_{sh}(t, t_c) = \varepsilon_{shu}\, \beta(h)\beta(t - t_c) \qquad (2.20).$$

Where ε_{shu} is the ultimate shrinkage strain, $\beta(h)$ is a correction term for the effect of humidity, and $\beta(t - t_c)$ is a correction term for the effect of time of drying.

The ultimate shrinkage ε_{shu} is given by equation (2.21).

$$\varepsilon_{shu} = 900k \left(\frac{30}{f_{cm28}}\right)^{0.5} 10^{-6} \qquad (2.21).$$

Where f_{cm28}, is the concrete mean compressive strength at 28 days in MPa and k is a shrinkage constant that depends on the cement type (Table A.12). If test results for strength development are available, the shrinkage term can be improved by interpolating k from Table A.12 using the experimentally determined cement type/characteristic.

The correction term for the effect of humidity $\beta(h)$ is given by equation (2.22).

$$\beta(h) = (1 - 1.18h^4) \qquad (2.22).$$

Note that for a relative humidity of 0.96, there is no shrinkage. At higher relative humidity, swelling occurs.

The time function for shrinkage $\beta(t - t_c)$ is given by equation (2.23).

$$\beta(t - t_c) = \left\{\frac{(t-t_c)}{(t-t_c)+0.12(v/s)^2}\right\}^{0.5} \qquad (2.23).$$

Where t and t_c are the age of concrete and the age drying starts or end of moist curing in days, respectively, and v/s the volume-surface ratio in mm.

2.7 Summary of Concrete Shrinkage Prediction Models and Recommendations

The comparison of shrinkage (Figure 2.5) clearly shows that the B-3 model neither overestimates like GL2000 model nor underestimate like CEB-FIB model rather it is an average and in between. Shrinkage deformation is too complex to be represented by a single mathematical expression. It has to be a combination of a few, and formulation based on pure mathematical functions is almost impossible. Thus incorporation of empirical coefficients is required in the development of prediction models for better accuracy.

Based on the three prediction methods discussed above, it is observed that both intrinsic and extrinsic parameters are equally important in influencing the magnitude of shrinkage strain in concrete. The main parameters considered are concrete mechanical properties, effective section thickness, and ambient relative humidity.

For most prediction equations, it can be summarized that the hyperbolic power function is adopted as the basis for most models because they function best reflect the pattern of shrinkage deformation over time. In addition to that, most prediction models propose correction factors to widen the range of concrete applications.

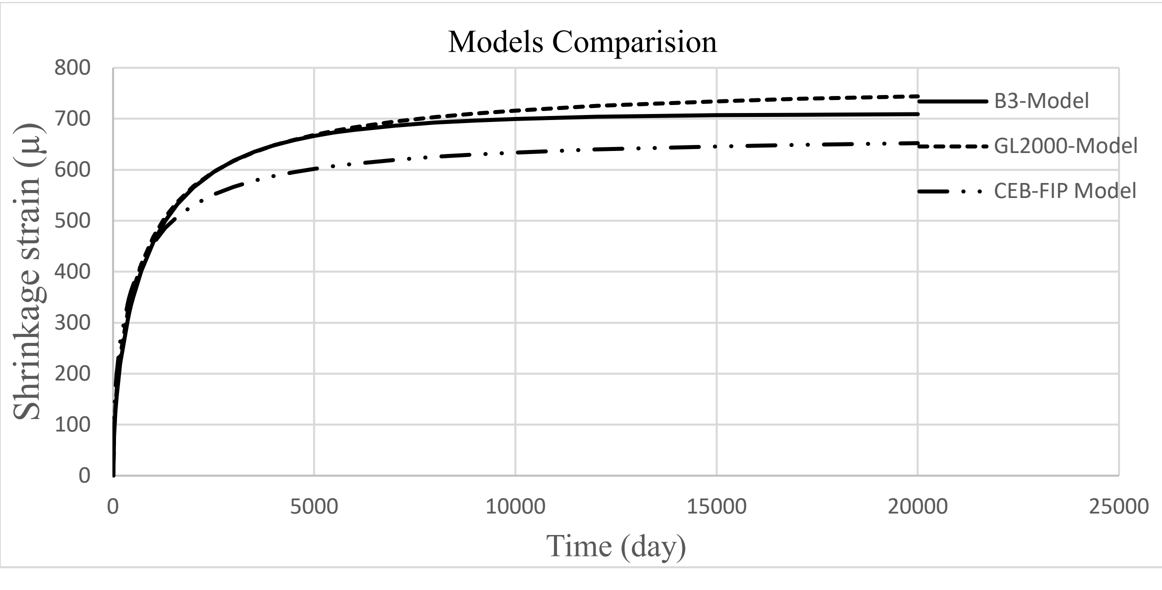

Figure 2. 5 Comparison curve of shrinkage models for long drying time.

2.8 Materials and Components

Reinforced concrete is a composite material, consisting of steel and concrete. However, concrete is in its turn also a composite material and can simply be seen as a composite of cement paste and aggregates. To understand and interpret the overall behavior of reinforced concrete, it is important to first understand the behavior and characteristics of each component (Fabian Narin and Olle Wiklund, 2012).

2.8.1 Concrete materials

Concrete is a composition of cement, water, and aggregates where the cement and water react and create a hardened cement paste, HCP. The aggregates consist of a graded rock material, which is contained inside the HCP and together they form the concrete material (Fabian Narin and Olle Wiklund, 2012). Most concretes used are lime-based concretes such as Portland cement concrete or concretes made with other hydraulic cement, such as cement fondue. However, asphalt concrete, which is frequently used for road surfaces, is also a type of concrete, where the cement material is bitumen, and polymer concretes are sometimes used where the cementing material is a polymer (Mala Babagana and Ani Abdulfatah, 2017).

Concrete has relatively high compressive strength, but significantly lower tensile strength, and as such is usually reinforced with materials that are strong in tension (often steel). Most concrete is poured with reinforcing materials (such as rebar) embedded to provide tensile strength, yielding reinforced concrete. The elasticity of concrete is relatively constant at low stress levels but starts decreasing at higher stress levels as matrix cracking develops. Concrete has a very low coefficient of thermal expansion, and as it matures concrete shrinks. All concrete structures will crack to some extent, due to shrinkage and tension (Mala Babagana and Ani Abdulfatah, 2017).

2.8.2 Reinforcement steel

Steel is the most commonly used material for the reinforcement of structural concrete. Normally the steel is regarded as linear until it reaches its yield capacity, where the material starts to behave non-linearly due to plastification (Fabian Narin and Olle Wiklund, 2012). Steel reinforcement is used to provide strength, ductility, and serviceability to concrete structures. Concerning serviceability, reinforcement is used to reduce instantaneous and long-term deformations and provide crack control (Nejadi, 2005).

2.8.3 Insulating polystyrene interface

Insulating polystyrene interface is the interlayer friction characteristics between a concrete slab and various types of sub-bases, which are commonly used in concrete slab-on-ground (Jin-Hoon Jeong *et al*.,2014). A plastic sheet between the slab and supporting soil minimize friction and moisture transportation (Øverli, 2014).

CHAPTER THREE

MATERIALS AND METHODS

3.1 General

As mentioned earlier the primary goal of this study is the analysis of shrinkage of a reinforced concrete slabs-on-ground by using a general-purpose finite element software, ABAQUS/CAE 2018 with the different parametric studies. This chapter is dedicated to describing the finite element method and modeling of material properties for both shrinkages and load analysis, for concrete, reinforcement, and ground interface.

3.2 Materials

Materials used in this study are concrete, reinforcement, load plate, and gravel interface layer between slab and ground. These materials were modeled and assigned for their corresponding part in Abaqus to perform an exact analysis and well-simulate the assembled model.

3.2.1 Concrete modeling

The concrete is modeled with the brick elements available in ABAQUS/CAE. Eight noded brick elements, C3D8R (Cube Three Dimensional Eight-node Reduced integration) element is used in the concrete part. These elements use linear interpolation in each direction and are often called linear elements of first-order elements. Moreover, these elements have only three degrees of freedom and are stress/displacement elements. Quadrilaterals have a better convergence rate than triangles and tetrahedrons, and sensitivity to mesh orientation in regular meshes is higher.

To represent the nonlinear behavior of concrete, the concrete damage plasticity (CDP) model available in ABAQUS has been employed. The damage parameters are calculated by considering the first tangent modulus of elasticity in the stress-strain curve obtained from the experimental test carried out in the laboratory.

The input parameters required for the defining concrete material model are: the uniaxial compression stress-strain curve; the uniaxial tension stiffening stress-strain curve, the volumetric dilation angle Φ, the eccentricity, the ratio of initial equibiaxial compressive yield stress to initial uniaxial compressive yield stress (fbo/fco) and the ratio of the tensile to compressive meridian (K) and viscosity parameter. These input parameters for the model are defined in Table 3.1 and uniaxial compressive and tensile loading responses for typical concrete grade of C30/37 are presented in Figure 3.1 as shown below.

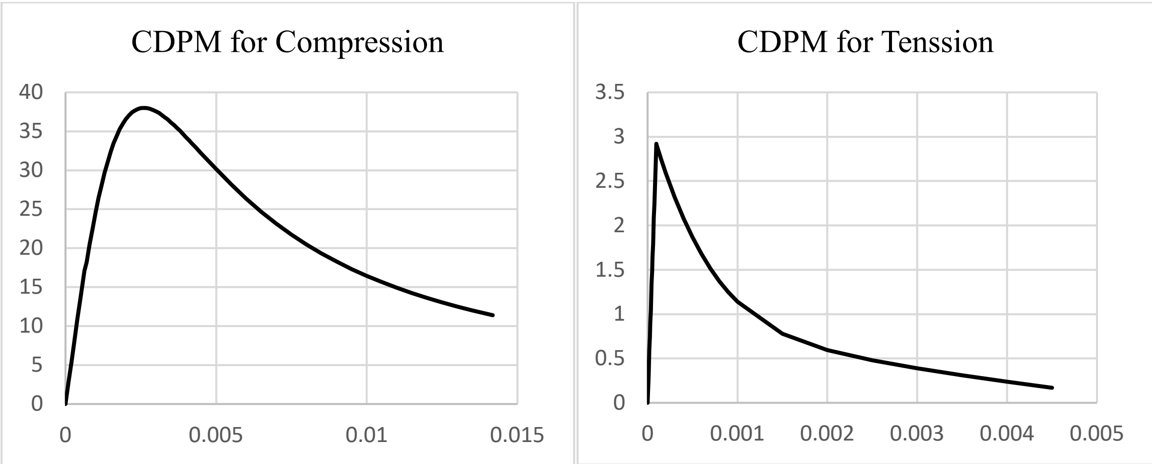

Figure 3. 1 Response of concrete C30/37 to uniaxial loading.

Table 3. 1 CDPM parameters for typical C30/37 concrete.

Compressive behavior			Tensile behavior		
Yield stress(MPa) (σ_c)	Inelastic strain $(\varepsilon_c^{\sim in})$	Damage parameter (d_c)	Yield stress(MPa) (σ_t)	Cracking strain $(\varepsilon_t^{\sim ck})$	Damage parameter (d_t)
17.10006	0	0	2.920334	0	0
18.198	3.49E-05	0.049815	2.904467	2.53E-06	0.002102
20.46014	5.22E-05	0.065238	2.746003	5.79E-05	0.047943
22.59453	7.42E-05	0.082421	2.596345	0.000113	0.093139
24.59174	0.000101	0.101182	2.322253	0.000222	0.180503
26.44473	0.000133	0.121324	2.079665	0.00033	0.262631
29.70207	0.000214	0.164924	1.865929	0.000437	0.338735
35.26275	0.000511	0.283978	1.514348	0.000649	0.472051
37.02514	0.000747	0.355594	1.24696	0.000858	0.581317

37.99993	0.001211	0.465815	1.138966	0.000962	0.627814
37.0892	0.001844	0.576377	0.779128	0.001474	0.795707
34.25779	0.002748	0.686973	0.59377	0.00198	0.889117
28.17015	0.00447	0.812799	0.479712	0.002484	0.940189
20.47543	0.007252	0.906454	0.39086	0.002987	0.967856
15.65391	0.009928	0.94551	0.311026	0.00349	0.982761
13.0482	0.012023	0.961848	0.237036	0.003992	0.990765
11.40039	0.013763	0.970615	0.169951	0.004494	0.995055

Density (tone/mm^3)	Modulus of elasticity (MPa)	Poisson's ratio	Coefficient of expansion (1/ºC)	Dilation angle	Eccentricity	fbo/fco	K	Viscosity parameter
2.40E-09	29799	0.2	1.00E-05	13	0.1	1.16	0.667	0.01

3.2.2 Reinforcement modeling

Reinforcing Steel rebars are modeled as three-dimensional truss elements (T3D2). A two-node straight truss element, that uses linear interpolation for position and displacement, has constant stress. It is defined that the cross-sectional area associated with the truss element is a part of the section definition. When truss elements are used in large displacement analysis, the updated cross-sectional area is measured by assuming that the truss is made of an incompressible material, regardless of the actual material definition. The orthogonal reinforcement grid is modeled as embedded reinforcement and represented by a bi-linear elastic perfectly-plastic material model (Figure 3.2) with a yield strength (σ_y) of 560 MPa. After yielding the reinforcement, plastic behavior was assumed with a 2% of strain hardening (Table 3.2).

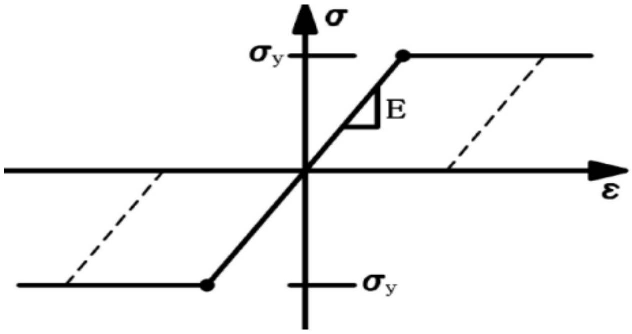

Figure 3. 2 Bi-linear stress-strain curve for reinforcement *(Prakash, 2018)*.

Table 3. 2 Elastic perfectly plastic mechanical property of reinforcement bar.

Yield stress (MPa)	Plastic strain	Modulus of elasticity (MPa)	Poison's ratio	Density (ton/mm^3)
560	0	200*10^3	0.3	7.85*10^{-9}
560	0.02			

3.2.3 Load plate modeling

To simulate the best possible experimental behavior, a loading plate of element type R3D4, which is constrained as a rigid body is modeled at the location of loading points. The tie constraint, having six nodal degrees of freedom, three translations, and rotations are defined between the loading plate and the top surface of the slab.

3.2.4 Interface layer and support modeling

The interface layer is modeled as an elastic shell element, having a 200 MPa modulus of elasticity and 0.3 poison's ratio as a gravel material. Friction characteristics, normal and tangential behaviors are assigned in the interaction module between a concrete slab and various types of sub-bases. Winkler springs are modeled as either elastic foundation with the modulus of elasticity, K_s (i.e 0.15 N/mm^3, (Øverli, 2014)) or spring/dashpot connect to the ground with spring stiffness, K_{si} (i.e 0.15*30*30 = 135 N/mm). Where 30mm is the mesh size of an interface element as shown in figure 3.3 below.

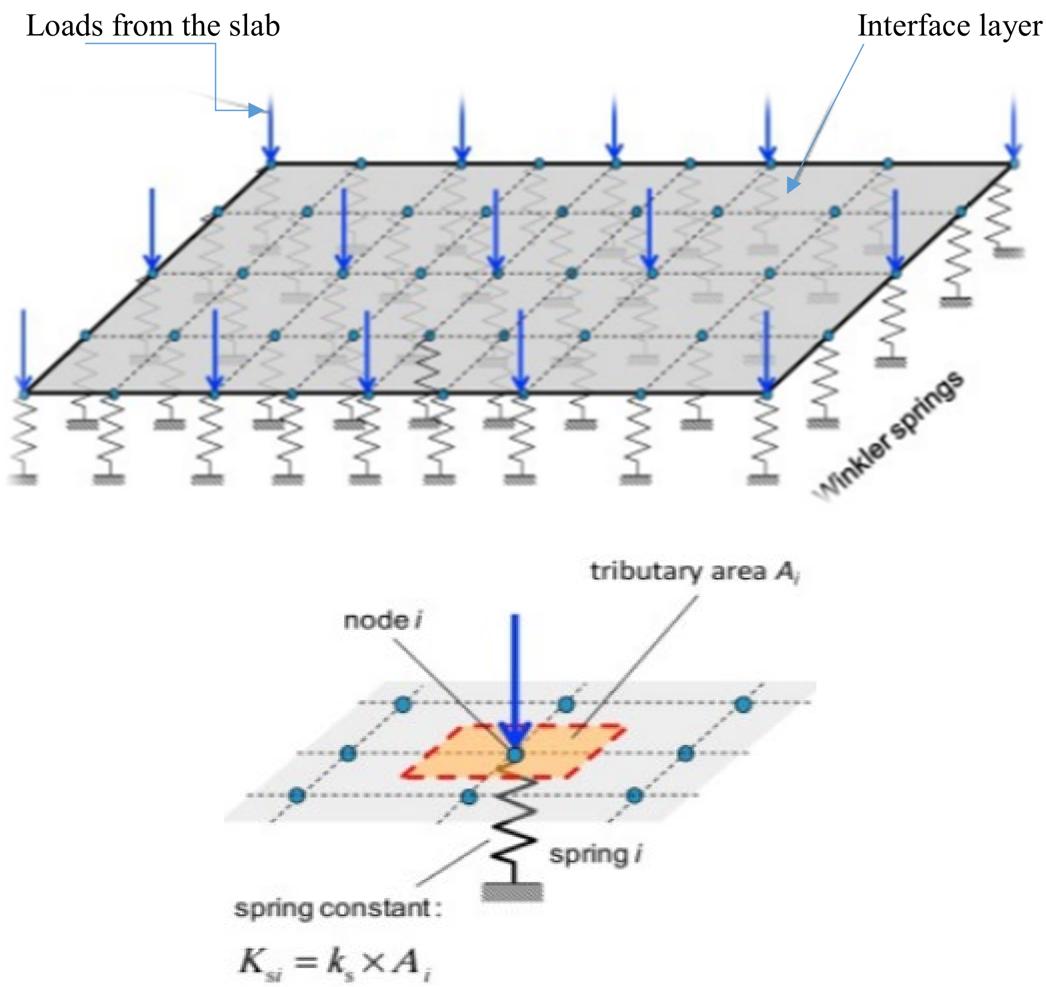

Figure 3. 3 Winkler springs as soil support for slabs-on-ground.

3.3 Methods

Non-linear finite element analysis of shrinkage of slabs-on-ground were analyzed using general-purpose software, ABAQUS/CAE, 2018. To investigate the influence of shrinkage of the slab-on-ground exposed to one side drying and to address the level of the tensile stresses, the 3D finite element analysis is used. A shrinkage profile depending only on slab thickness was implemented in ABAQUS using an equivalent temperature distribution (Desai, 2011). Low shrinkage strains were assigned to the lower half of the concrete slab, and an exponential strain profile is used (figure 3.4). Total shrinkage strain can be represented by equation (3.1), a third parameter was added in the equation because it allows modifying the shape of the profile more easily if ever it was needed to calibrate the shrinkage strain profile.

$$\mathcal{E}_{sh}(y) = a + b.e^{\lambda y} \quad (3.1).$$

Where $\mathcal{E}_{sh}$ is strain expressed in micro strains, y is slab height in mm, a, b and λ are constants obtained from the three shrinkage values (i.e bottom, top, and an arbitrary point). Where strain at top and bottom is an ultimate and from 0 to 25% of ultimate shrinkage respectively. The conditions were initially assumed for ultimate strains to fit with the shrinkage strain profile derived by (Desai, 2011). The temperature profile calculated in Table 3.3 is applied through the thickness of the slab as a predefined temperature field.

Table 3. 3 Shrinkage & equivalent temperature gradient through thickness.

Slab depth, y (mm)	Shrinkage strain (μ)	Equivalent temperature (ºC)
0	-35.45489	-3.54549
10	-39.00038	-3.90004
30	-51.59847	-5.15985
40	-62.41176	-6.24118
60	-100.8343	-10.0834
90	-250.9975	-25.0997
120	-708.976	-70.8976

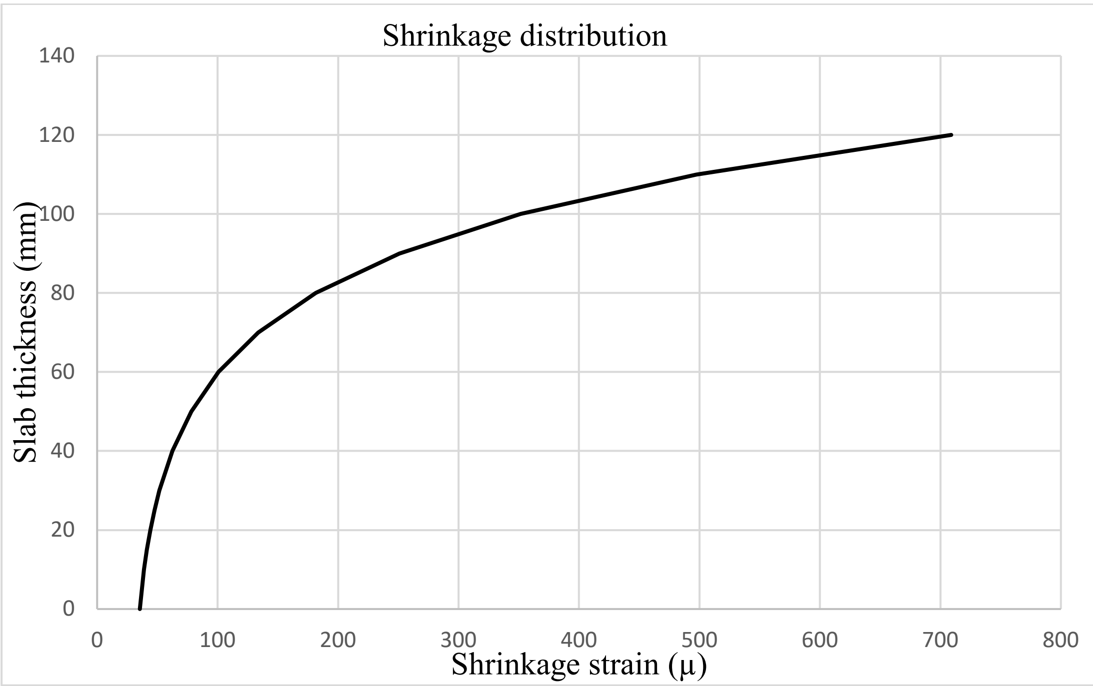

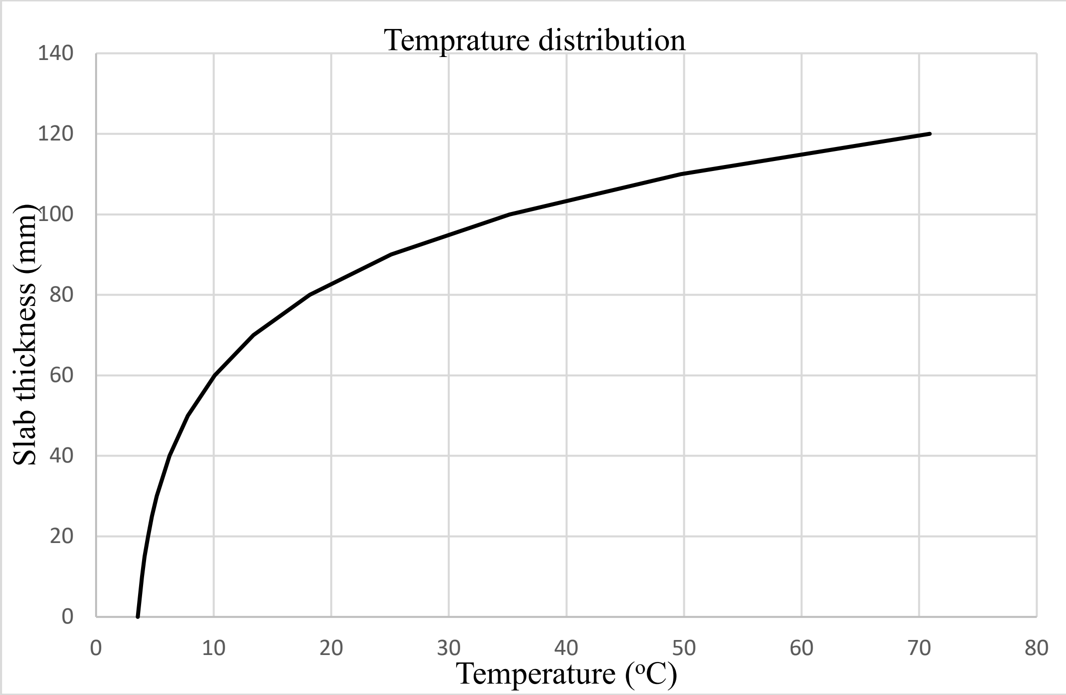

Figure 3. 4 Shrinkage strain & Temperature distribution across the slab thickness.

3.4 Finite Element Model and Validation

To verify the selected FE models in ABAQUS, the load versus displacement and shrinkage strain of the simulated models are compared with the case studies performed by (Øverli, 2014) and (Shideh Shadravan *et al*., 2015) respectively. The selected slabs are 3.5 m x 3.5m x 120mm for load versus displacement (Figure 3.5), and 915mm x 3048mm x 76mm for shrinkage strain verification (Figure 3.6) of slab-on-ground. The displacements for loads at the corner and edge of the slab as well as shrinkage strain of the slabs-on-ground were investigated.

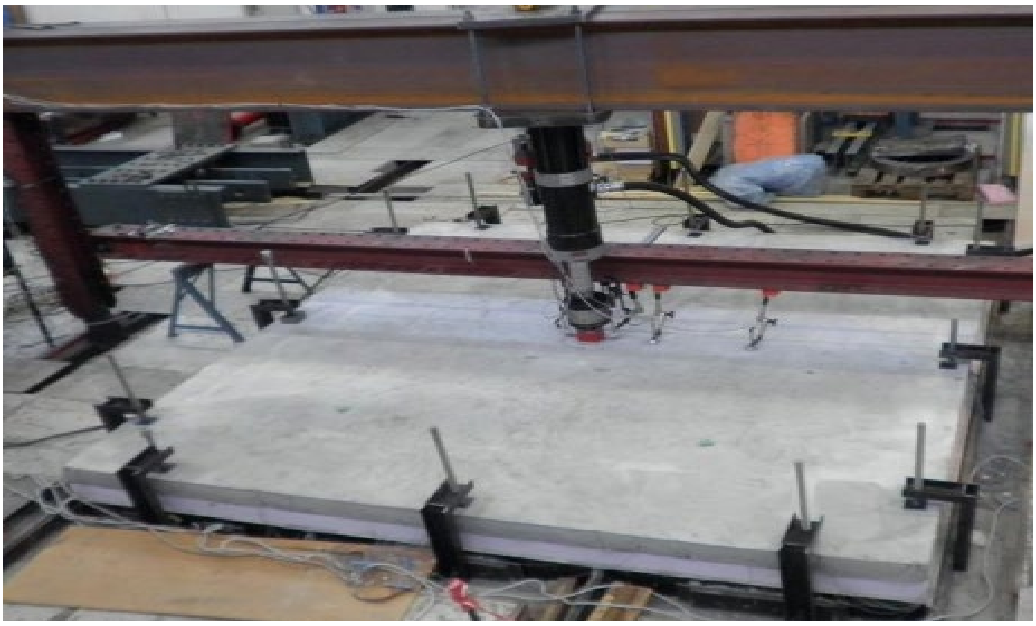

Figure 3. 5 Slabs-on-ground test set-up for load-deflection validation *(Øverli, 2014)*.

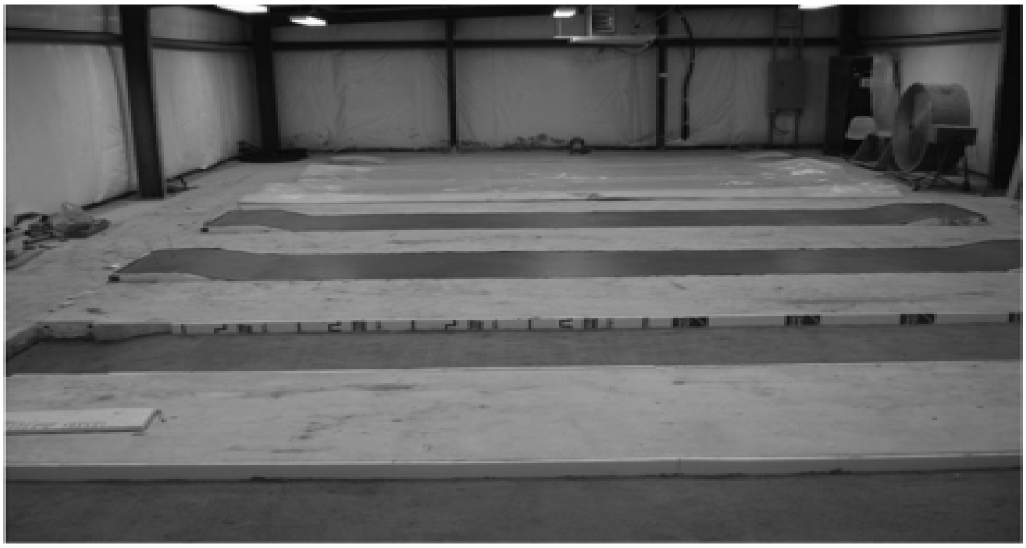

Figure 3. 6 Slab-on-ground test set-up for shrinkage validation (Shadravan *et al*., 2015).

3.6 Parametric Studies

Investigation of shrinkage strain, deformation, tensile damage, and maximum principal stress for varying slab size and thickness, concrete strength class, the position of reinforcement, relative humidity, modulus of subgrade, boundary conditions, the frictional effects between the slab and sub-base, and effects of external loads which tabulated in Table 3.4, are performed using general-purpose software, ABAQUS/CAE 2018.

Table 3. 4 Parameters used in shrinkage analysis of slabs-on-ground.

Parameters	Quantity	Unit	Remark
Slab length	3500x1500x120	mm^3	One way slab
	3000x2000x120	mm^3	Two way, rectangular "
	3000x3000x120	mm^3	Two way, square "
Slab thickness	80	mm	
	120	mm	
	160	mm	
Concrete grade	C20/25	MPa	
	C25/30	MPa	
	C30/37	MPa	
Reinforcement Position	Plain concrete	MPa	S560
	Only bottom bar	MPa	S560
	Only middle bar	MPa	S560
	Both top & bottom bar	MPa	S560
Relative humidity	40	%	
	60	%	
	80	%	
Modulus of subgrade	0.05	N/mm^3	
	0.1	N/mm^3	
	0.15	N/mm^3	
Friction	0		Frictionless
	0.3		
	0.5		
Boundary condition	All ends free		Unrestrained
	All ends restrained		
	The adjacent ends " "		
load	Center load	20,000N	
	Corner load	20,000N	
	Shorter edge load	20,000N	
	Longer edge load	20,000N	

CHAPTER FOUR

RESULTS AND DISCUSSIONS

4.1 Introduction

The deflection, stress, and damage of slabs-on-ground subjected to nonlinear shrinkage strain distribution were studied using the FEM. The FE model was first verified by comparing the deflection and shrinkage strain of the simulated slabs-on-ground with those of experimental studies. Firstly, the FE study of the slabs-on-ground was validated for both deflection and shrinkage strain, and results were compared. From validation of shrinkage strain and displacement, ABAQUS/CAE 2018 gives us an excellent agreement with the test results. Secondly, the results for the parameters and studies were discussed. The last results were discussed briefly and well summarized.

4.2 Finite Element Validation Results

The results of experiments were compared with the FEA results; the values are shown for comparison in Figure 4.1 and figure 4.2 for displacement and shrinkage respectively. The shrinkage strain of slab-on-ground measured at the top surface of the slab and displacements were investigated at two locations, edge and corner of the slabs-on-ground. Good agreement was obtained for shrinkage strain and load-displacement models.

The results show that the FEA prediction of shrinkage strain (variation with 1.1%) and displacement (Figure 4.1) agrees very well with the experimental results. This comparison served to confirm that the modeling techniques employed for the study were valid.

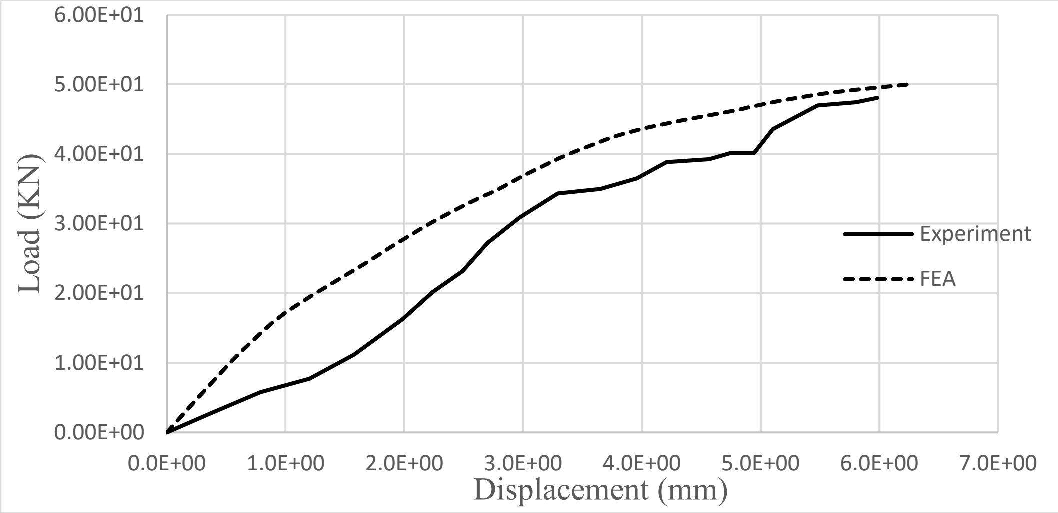

(a).

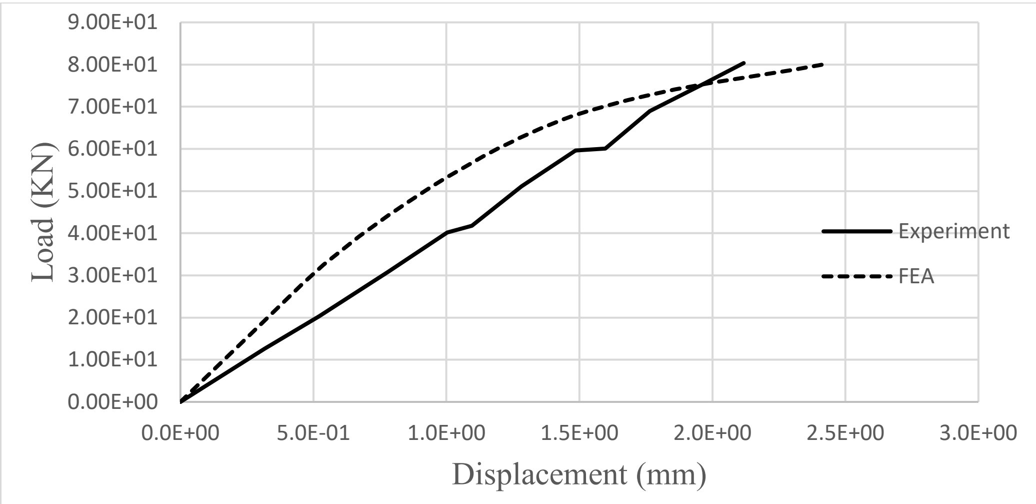

(b).

Figure 4. 1 Load-displacement validation curves for corner (a), & edge (b) loads.

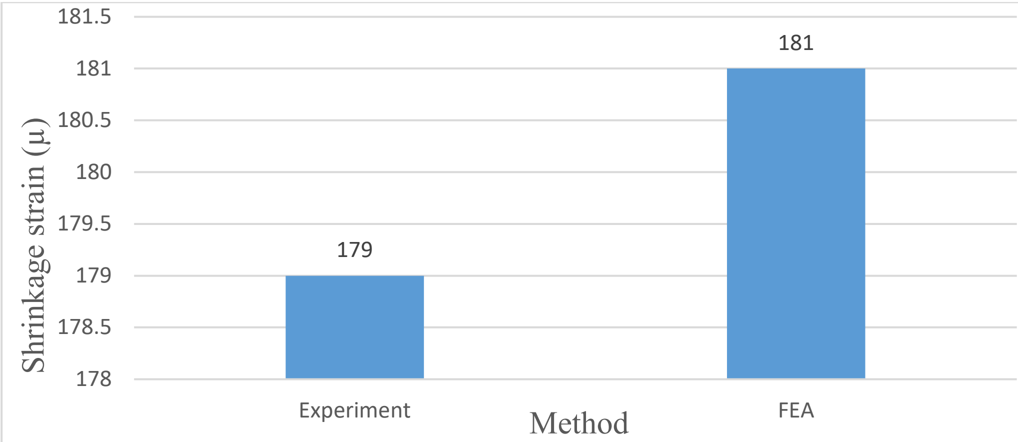

Figure 4. 2 Shrinkage strain validation of slab-on-ground.

4.3 Parametric Studies for Shrinkage Analysis of Slabs-on-Ground

Parametric studies were performed to analyze the effects of key parameters on the deformation, maximum principal stress, and tensile damage formation in the slabs-on ground model, restrained at the sub-base and subjected to gradient shrinkage. Key parameters (section 3.6) were analyzed and discussed in the upcoming sections. Two finite element models have been analyzed. In the first model, the outer edges of the slab are free to move vertically and parameters are studied while the second model is supported to avoid vertical deformations at the edges (Figure 4.18).

Typical analysis results presented (from Figure 4.3 to Figure 4.8) for typical slab size 3000mmx2000mmx120mm (length x width x thickness), with concrete strength class C30/37, having S-560 (yield strength f_y = 560 MPa) reinforcement bar in both top and bottom of concrete slab, coefficient of friction (μ) 0.3. From Figure 4.3 and Figure 4.4 (b) it can be seen that the corner will lift more than 1.1 mm and the center deflect downward more than 0.2 mm (Figure 4.4a) without the edge supports.

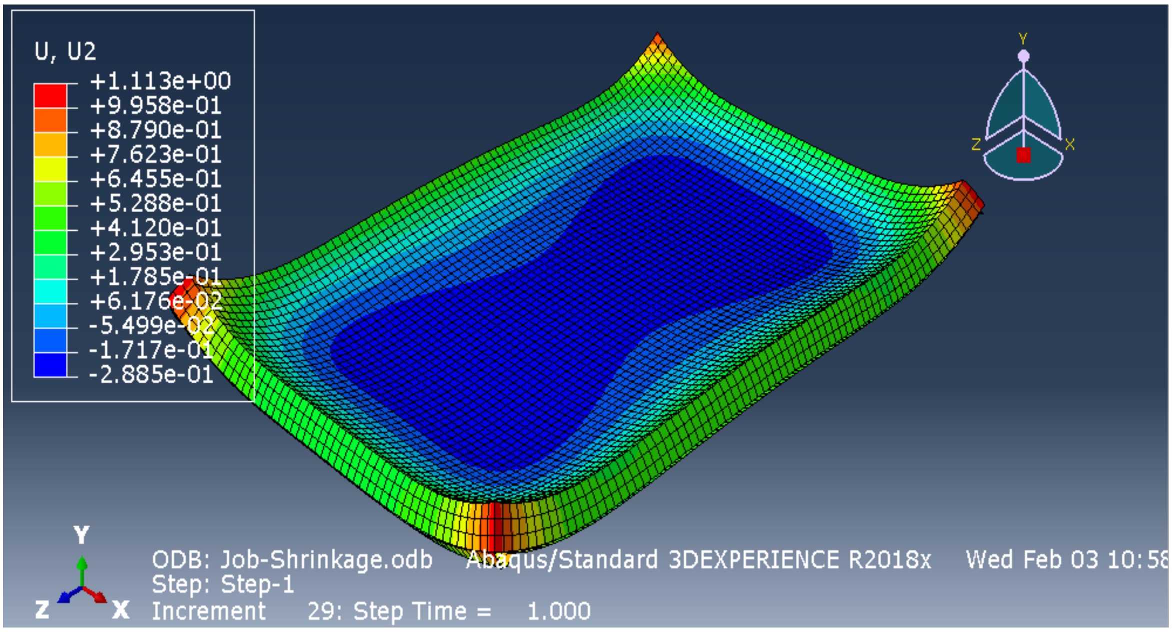

Figure 4. 3 Deformed shape of the slab for non-linear shrinkage strain distribution.

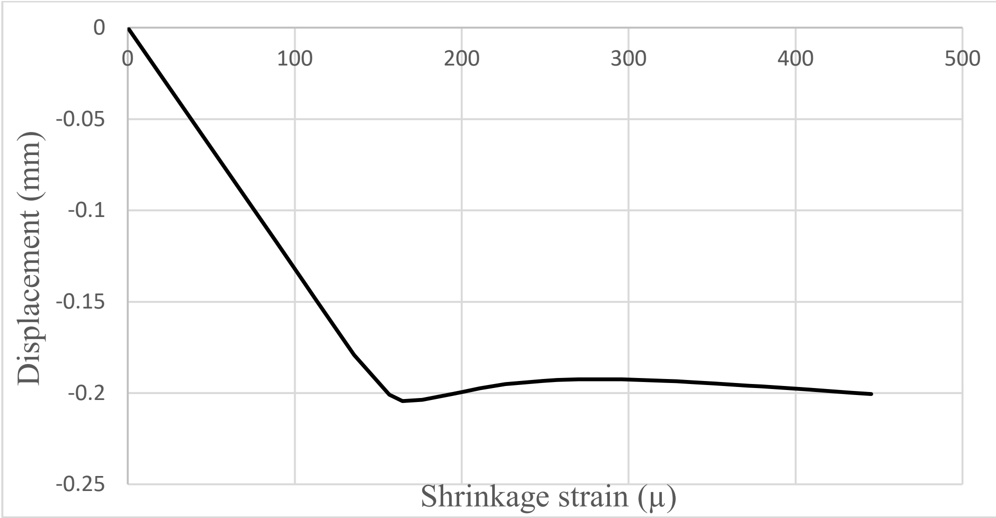

(a).

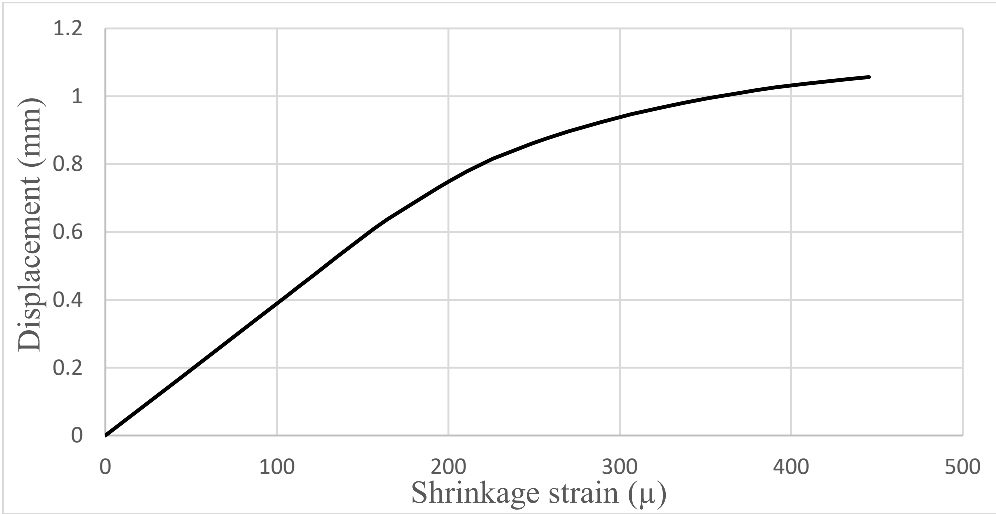

(b).

Figure 4. 4 Displacement-shrinkage strain curves at (a) center & (b) corner of the slab.

Figure 4.5 presents the principal stress distribution at the top surface for the slab model. The obtained maximum tensile stresses, 3.007 MPa, are 3-4 N/mm^2, which is in the range of the tensile strength of concrete; hence, the slab may crack due to drying shrinkage.

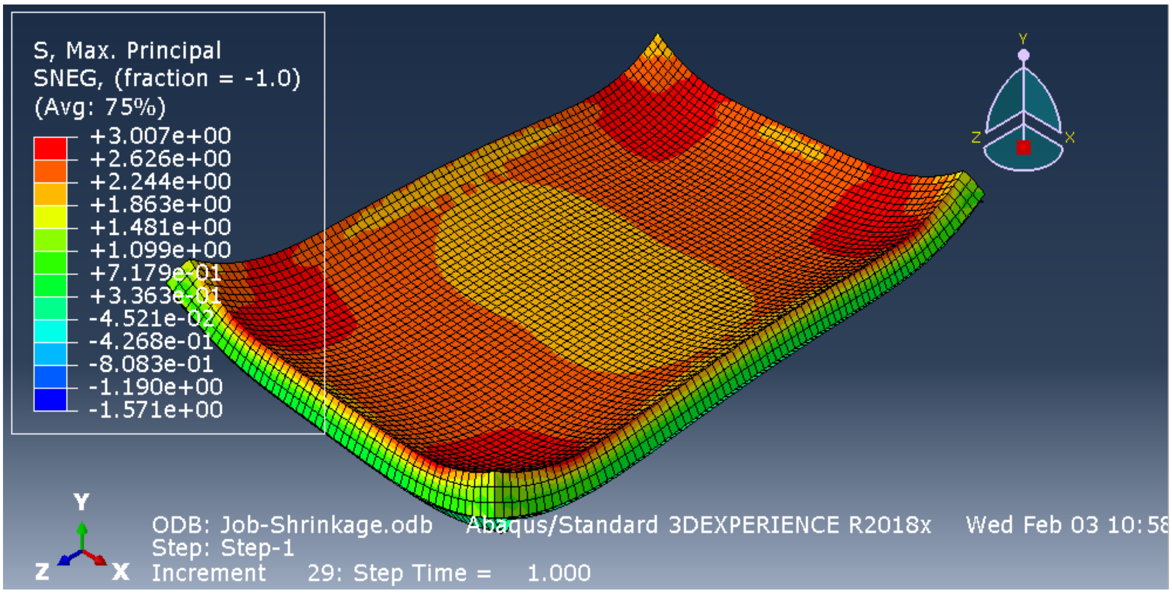

Figure 4. 5 Maximum principal stress of slab.

The maximum compression damage (Figure 4.6) was obtained as 0.186 along the edge surface of the slab and maximum tensile damage was 0.284 contoured as shown in Figure 4.7 which is an indication of cracking on the slab surface.

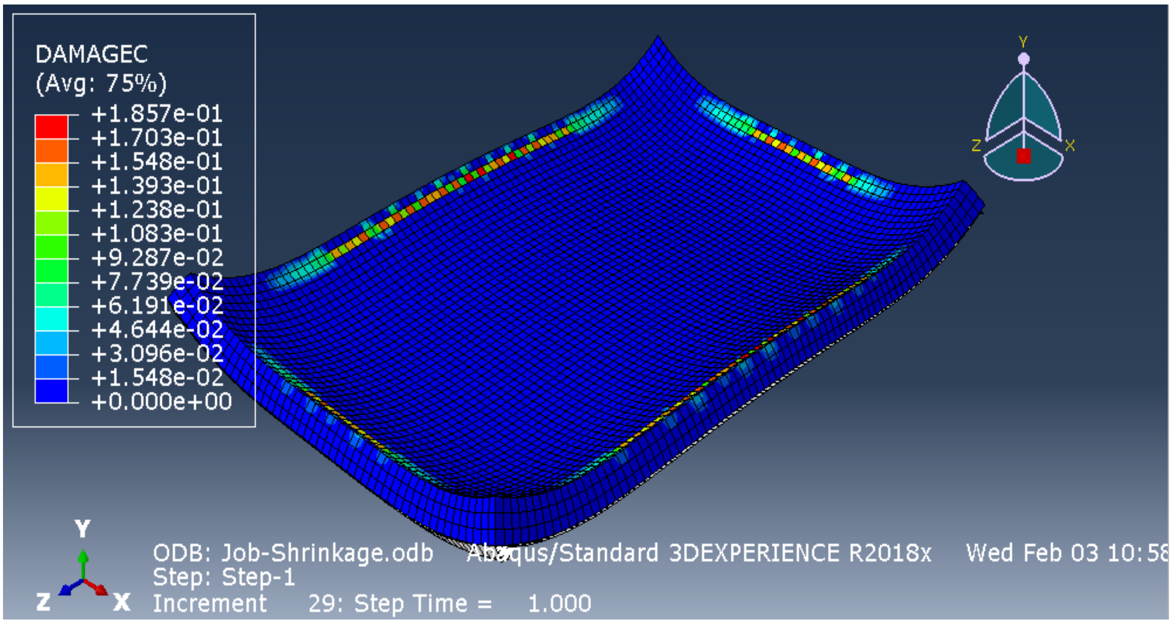

Figure 4. 6 Compression damage contour of the slab.

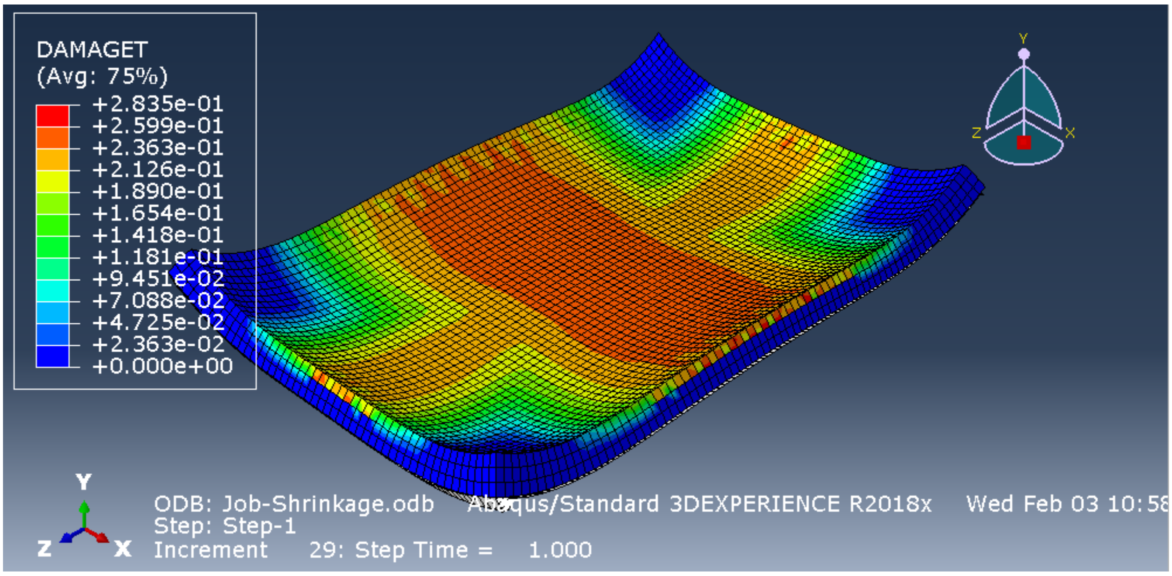

Figure 4. 7 Tensile damage contour of the slab.

The nonlinear shrinkage strain distribution was modeled as equivalent temperature distribution and thermal strain distribution across the depth of the slab was obtained in Figure 4.8 below which is equivalent to shrinkage strain distribution. As seen from Figure 4.8 maximum negative temperature gradient (i.e equivalent to maximum shrinkage strain) was obtained on the top surface of the slab and the bottom of the slab was subjected to minimum shrinkage strain.

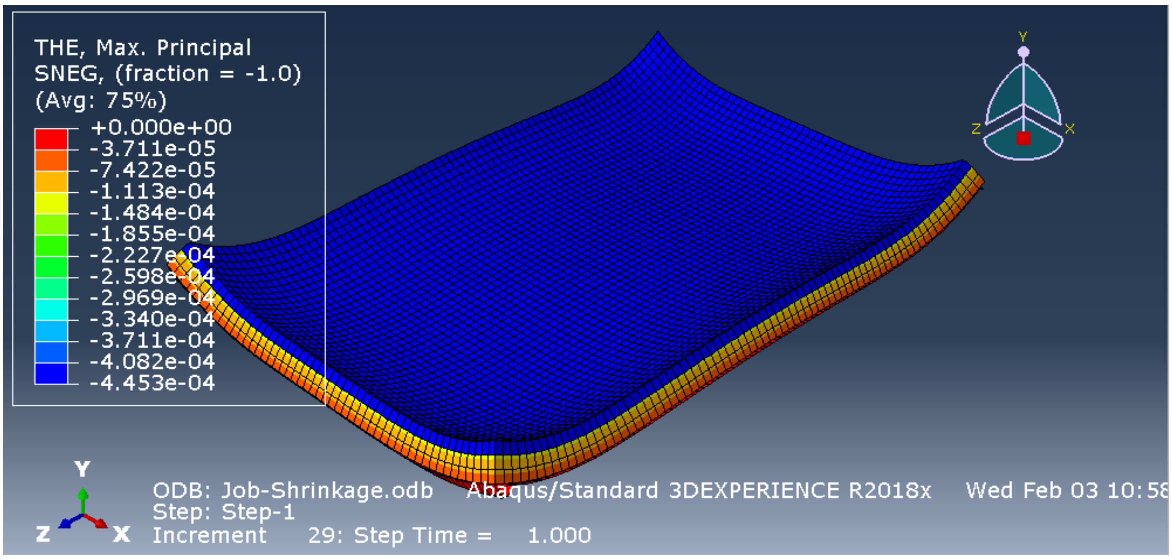

Figure 4. 8 Shrinkage strain distribution across thickness of the slab.

4.3.1 Slab sizes

Structural dimensions of the slabs influence the deformation, stress, and damage behavior. Vertical deflection and maximum principal stress responses for varying slab lengths are presented in Figures 4.9 (a) and (b) respectively, while other parameters are kept constant as shown in Table 3.3, section 3.6. As indicated in Figure 4.9 (a) and (b), the slab length influences the maximum vertical displacement and principal stress respectively, and maximum deflection and minimum principal stress were obtained for one-way slab size, and for the square slab, the reverse is true.

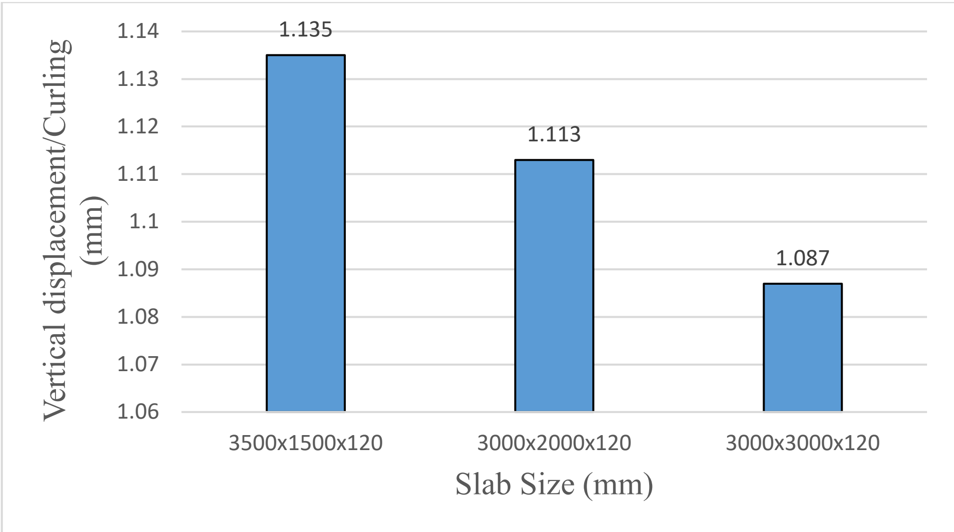

(a).

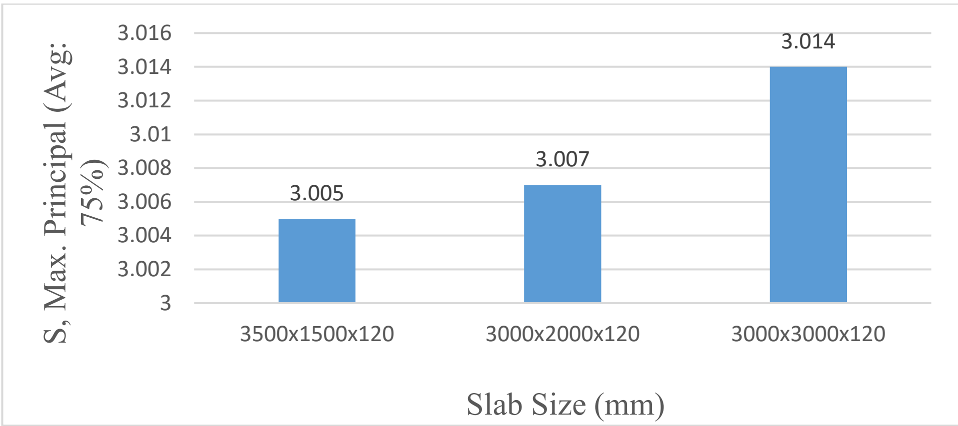

(b).

Figure 4. 9 Vertical displacements (a) & maximum principal stress (b) for slab sizes.

4.3.2 Slab thicknesses

The thickness of the slab varied from 80 mm to 160 mm, while other parameters were kept constant. The maximum deflection and tensile damage response were measured as a result of shrinkage strain. Thickness has a great influence on the maximum tensile damage development concerning applied shrinkage strain which results in high crack formation. It is evident from Figure 4.10 that the smaller the slab thickness the smaller the maximum vertical deflection and tensile damage. Vertical deflection and tensile damage (i.e crack formation) was higher as the slab thickness was increased as illustrated in Figure 4.10.

(a). 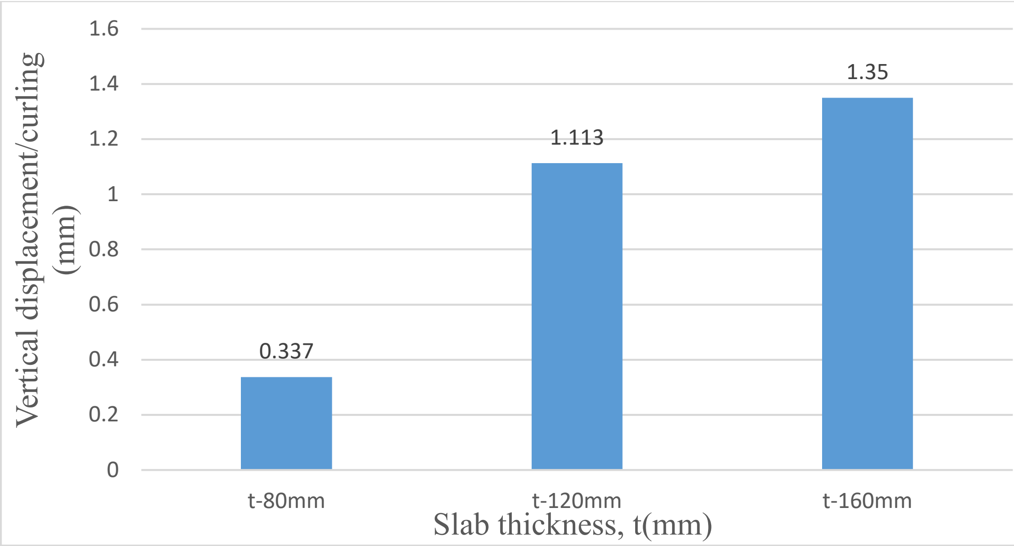

(b). 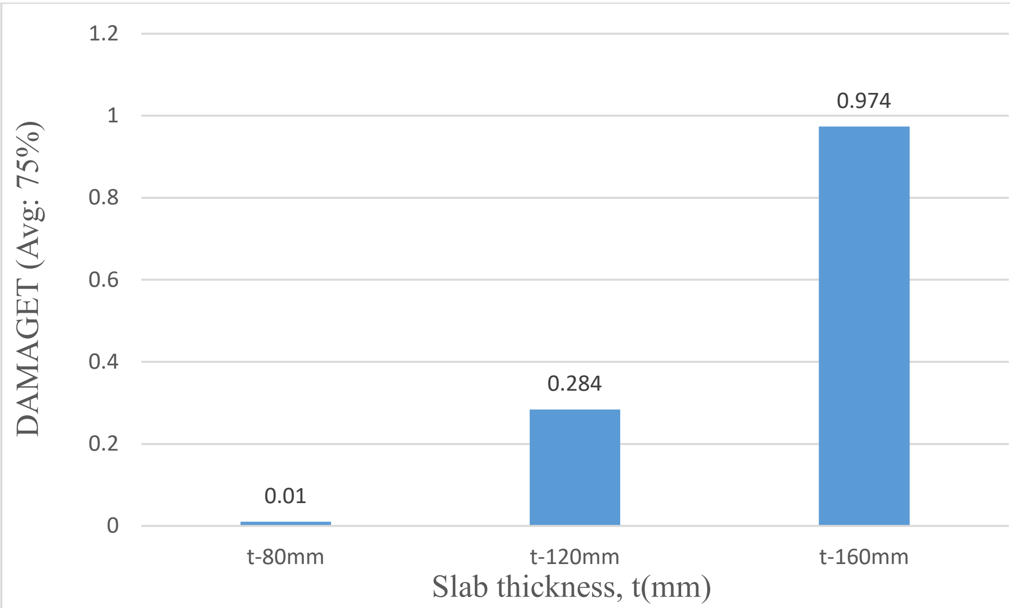

Figure 4. 10 Vertical displacements (a) & tensile damage (b) for slab thicknesses.

4.3.3 Concrete grades

Slabs with different concrete strength classes were investigated for shrinkage strain by considering the parameters listed in Table 3.4. The maximum vertical deflection and maximum principal stress values increase for increasing shrinkage strain as shown in Figure 4.11. For the concrete strength classes C20/25 and C25/30 the deformation is slightly lower than for C30/37.

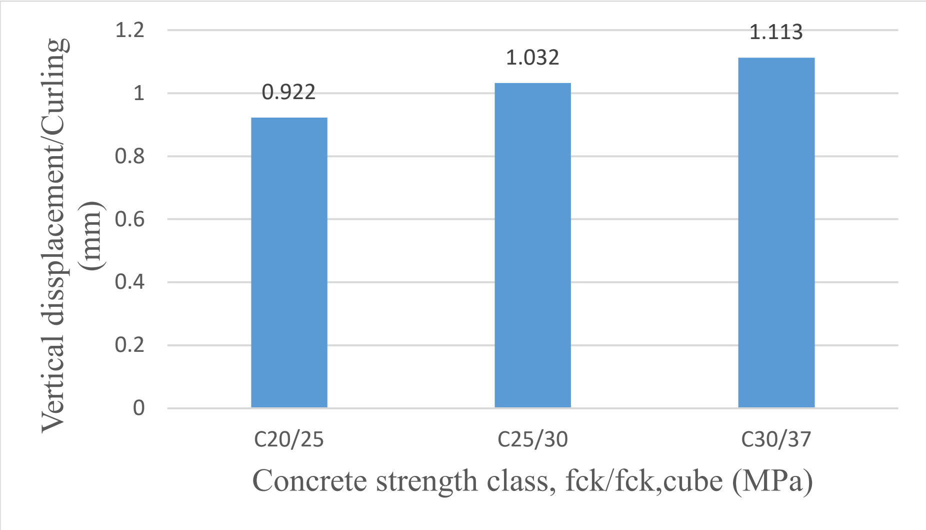

(a).

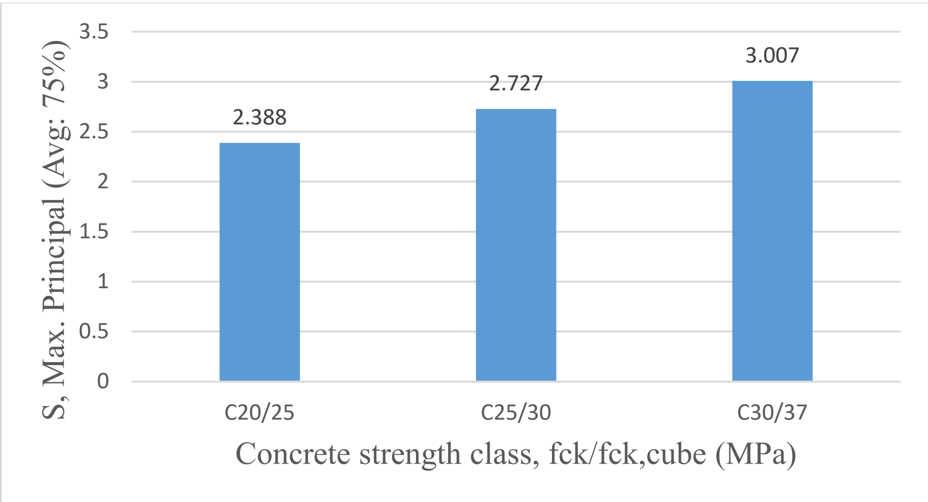

(b).

Figure 4. 11 Vertical displacements (a) & maximum principal stress (b) for concretes.

4.3.4 Reinforcement positions

The finite element models indicate that nearly the same maximum principal stress occurs at the mid-depth and bottom of the slab. For this reason, the crack control reinforcement in slabs-on-ground may be more effective if placed either at mid-depth or in the slab bottom as the latter is common in practice. The top reinforcement is in the most highly stressed part of the slab, making it efficient in controlling the spread of cracks due to tensile damage, and because of the reduced cover to the top of the slab, it would also improve its effectiveness in controlling surface crack widths.

Reinforcement position is one key parameter to control the crack formation and vertical deflection caused by shrinkage strain. Reinforcement position is varied through the thickness for the bottom, middle, and both top and bottom of the slab, keeping the concrete cover constant to 20 mm on both top and bottom side. The bar diameter was kept constant, 8mm, and all other parameters are listed in Table 3.4. Vertical deflection slightly reduces from only bottom reinforcement to plain concrete, Figure 4.12 (a). Maximum tensile stresses are nearly the same for the reinforcement bar at the middle and bottom of the slab and tensile damage is slightly reduced for middle reinforcement than bottom reinforcement position, shown in Figure 4.12.

(a).

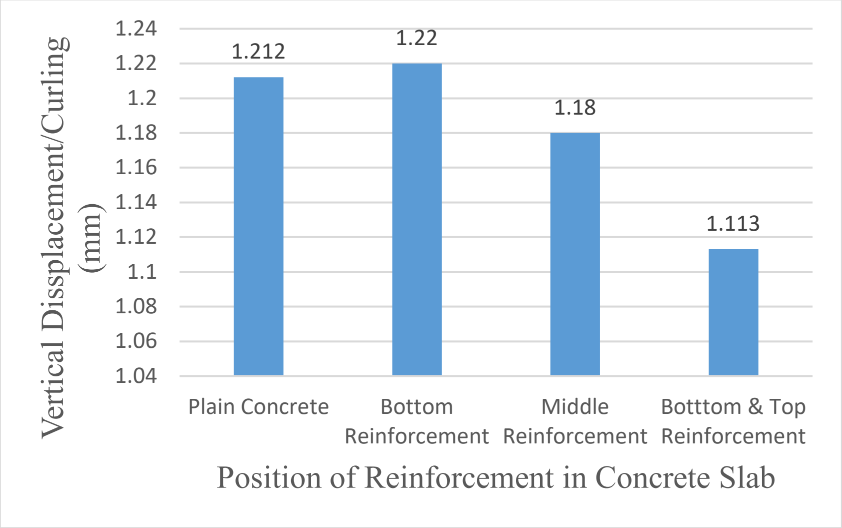

(b).

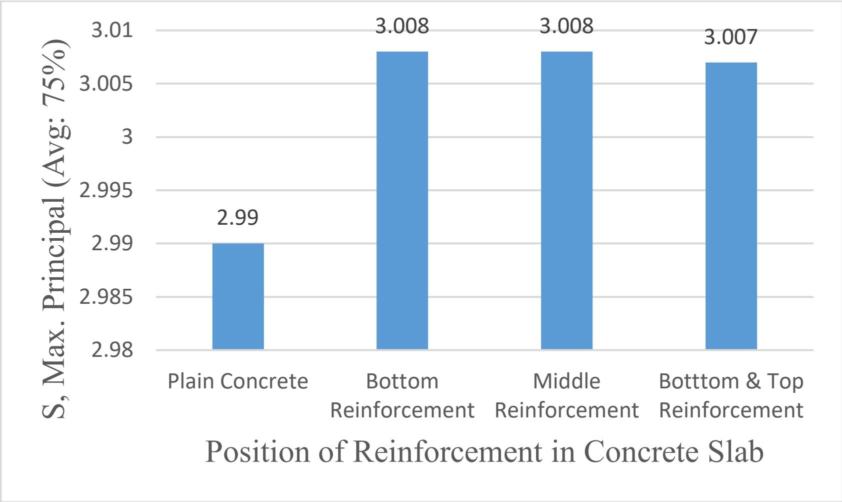

(c).

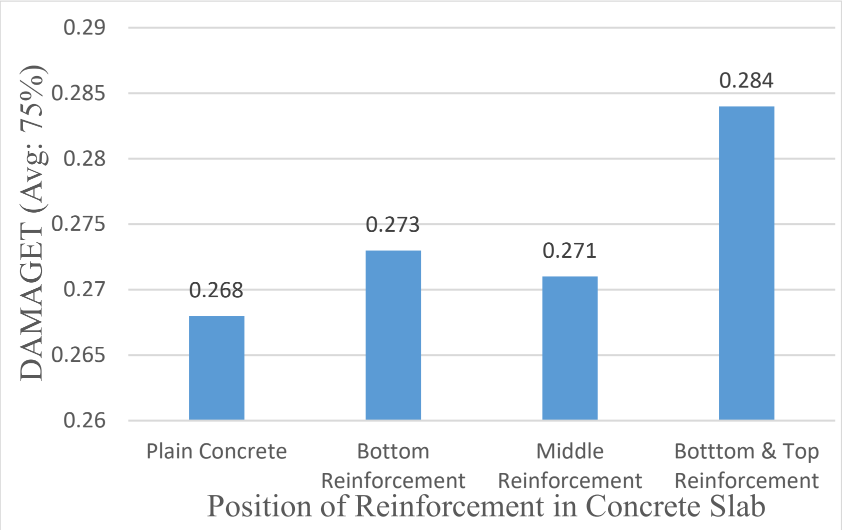

Figure 4. 12 Vertical displacements (a), maximum principal stress (b), and tensile damage (c) for different locations of the reinforcement bar.

4.3.5 Relative humidity

As relative humidity (RH) increases, shrinkage strain will be reduced so that vertical displacement also decreased (Figure 4.13a). Also, maximum principal stress decreases as relative humidity increases (Figure 4.13b). This is because as relative humidity increases, moisture on the concrete surface increases and drying will be decreased. Higher relative humidity in the ambient air at the upper surface will reduce the severity of curling even though the concrete may be a high shrinkage material.

(a). 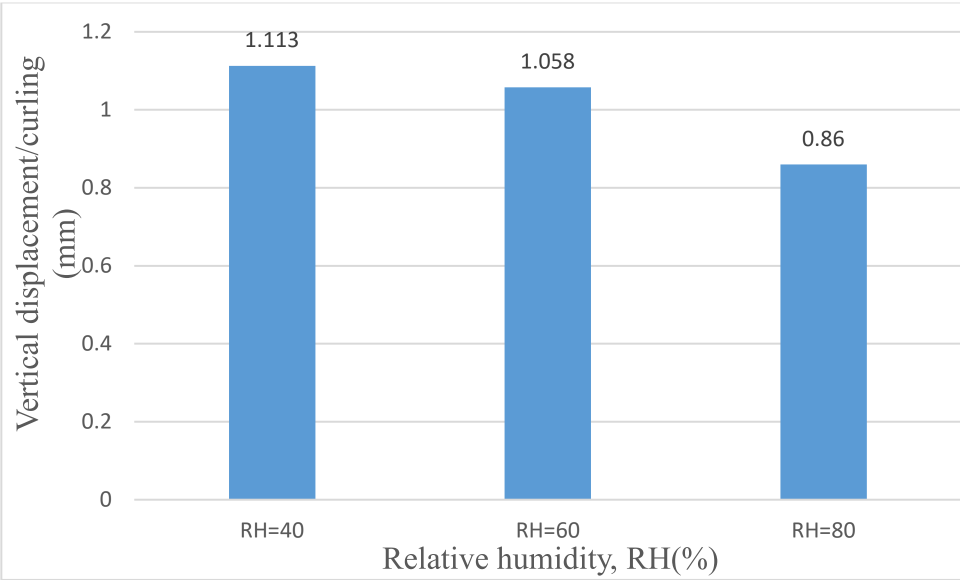

(b). 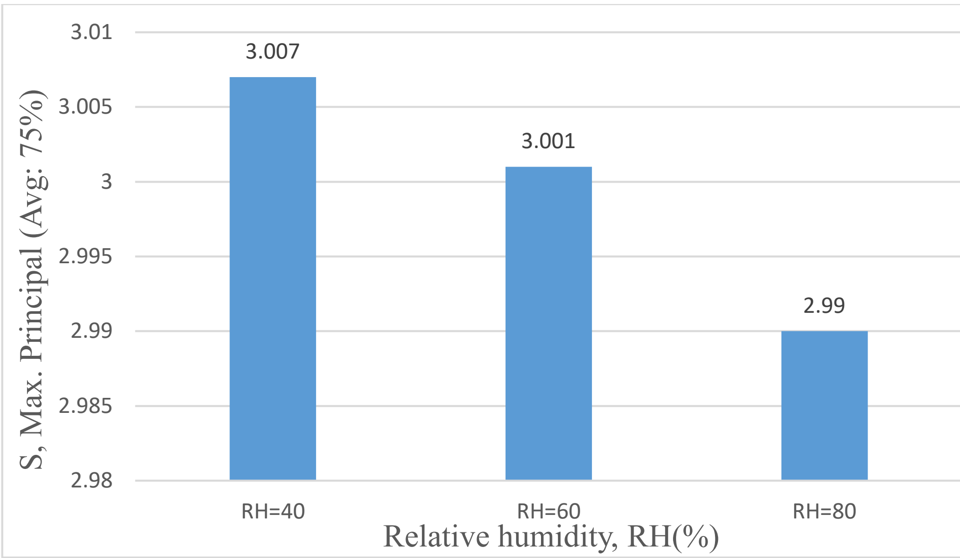

Figure 4. 13 Vertical displacements (a) & maximum principal stress (b) for RH.

4.3.6 Loads

Application of shrinkage to the concrete slab is performed in a single step (step-1) and load in the next step (step-2). The 20,000 N load was applied as an external load at the center, corner, shorter edge, and the longer edge of the slab together with the shrinkage strain. In Figure 4.14 the load (i.e both concentrated and shrinkage strain loads)-vertical deflection curves for the four cases are presented. Nonlinear deflections for increasing shrinkage strain and load were observed for all cases.

(a).

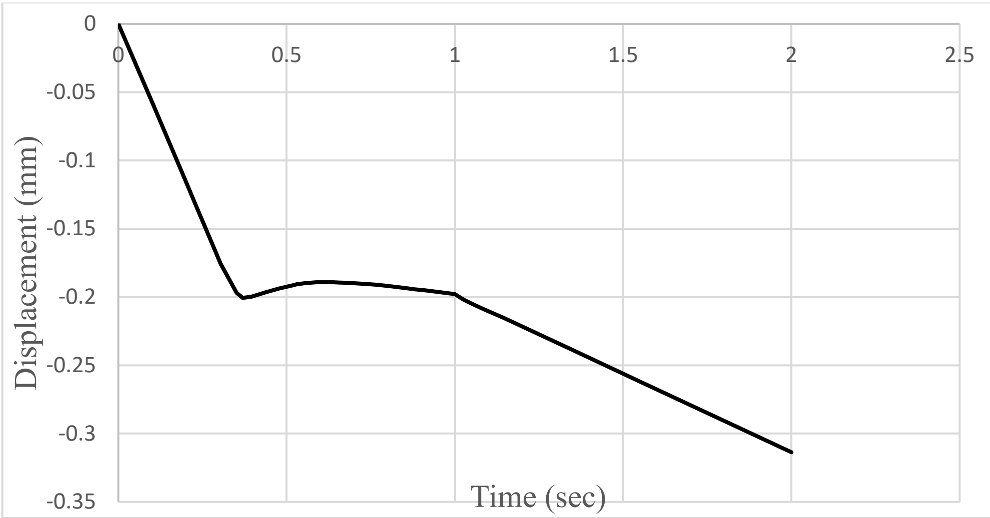

(b).

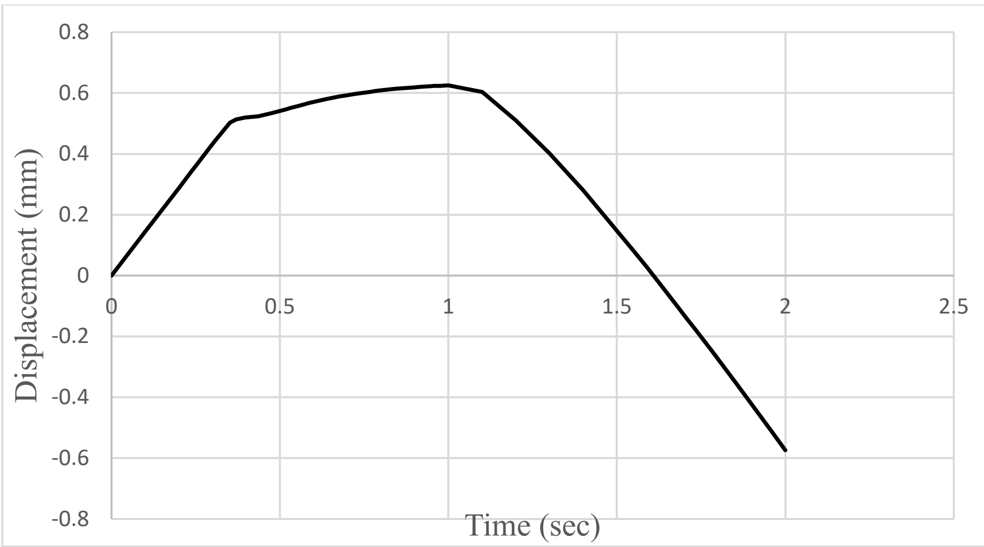

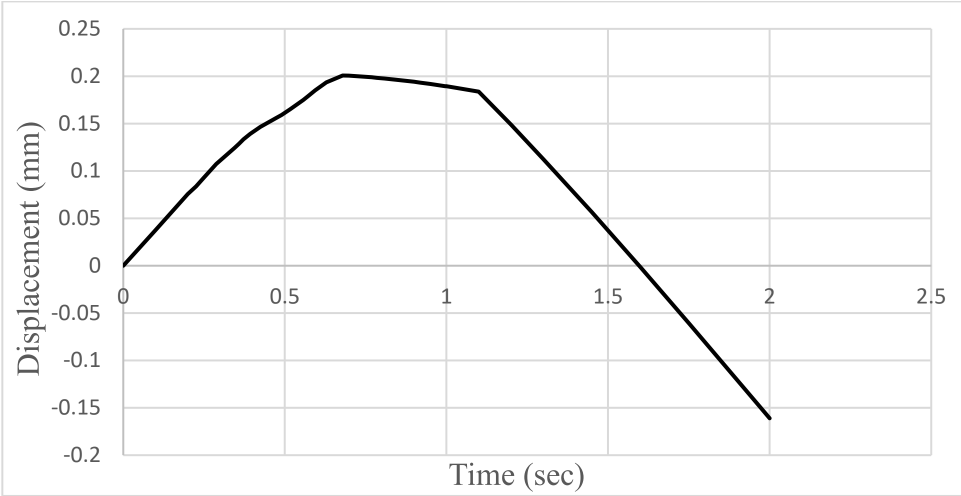

(c).

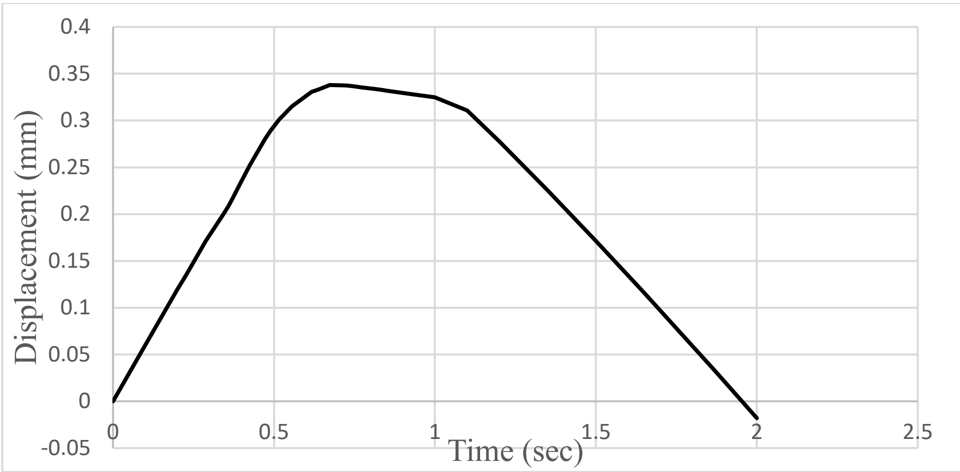

(d).

Figure 4. 14 Displacement - Time curves for both shrinkage strain and loads at (a) center, (b) corner, (c) shorter edge, and (d) longer edge.

4.3.7 Modulus of sub-grades

Subgrade stiffness for typical grounds varies from 0.01 N/mm^3 for fine sand to 0.5 N/mm^3 for well-compacted crushed stone. To investigate the effect of the stiffness on deflection due to shrinkage, the stiffness has been varied and compared with the obtained maximum vertical displacement. The result presented in Figure 4.15, shows that displacement decreases as sub-grade stiffness (modulus of subgrade) increases.

There are two alternatives available in ABAQUS/CAE to model Winkler's foundation, one Elastic foundation, and the other spring/dashpot connect to the ground. As seen in Figure 4.16 both models result in quite a similar deflection concerning shrinkage strain.

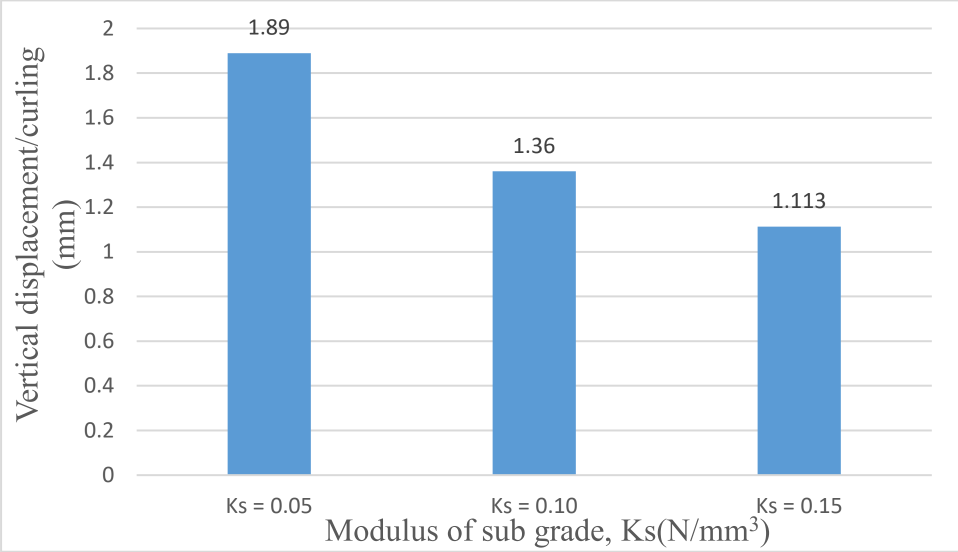

Figure 4. 15 Vertical displacement chart for different modulus of subgrade.

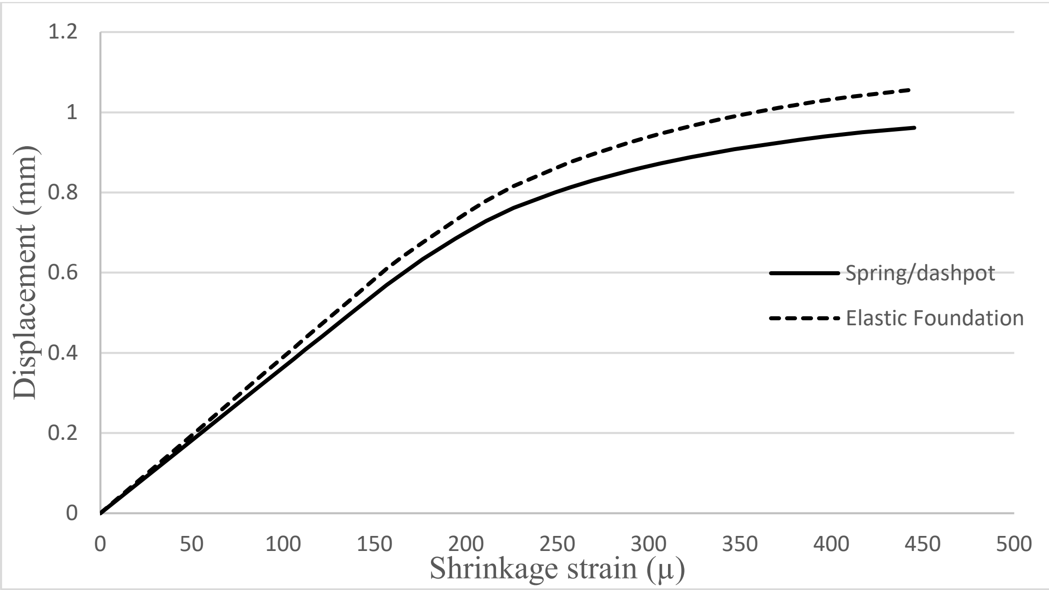

Figure 4. 16 Displacement-Shrinkage strain curve for different Winkler's spring model.

4.3.8 Frictions

In slabs on grade, the frictions from the ground restraints vertical displacement. However, if shrinkage is the only applied load together with a frictionless interface material model for the ground, there will be maximum principal stresses due to the free lifting of the slab (Figure 4.17). For friction coefficients (μ) of interface 0.3 and 0.5, there is almost similar deflection and stress as shown in Figure 4.17 below.

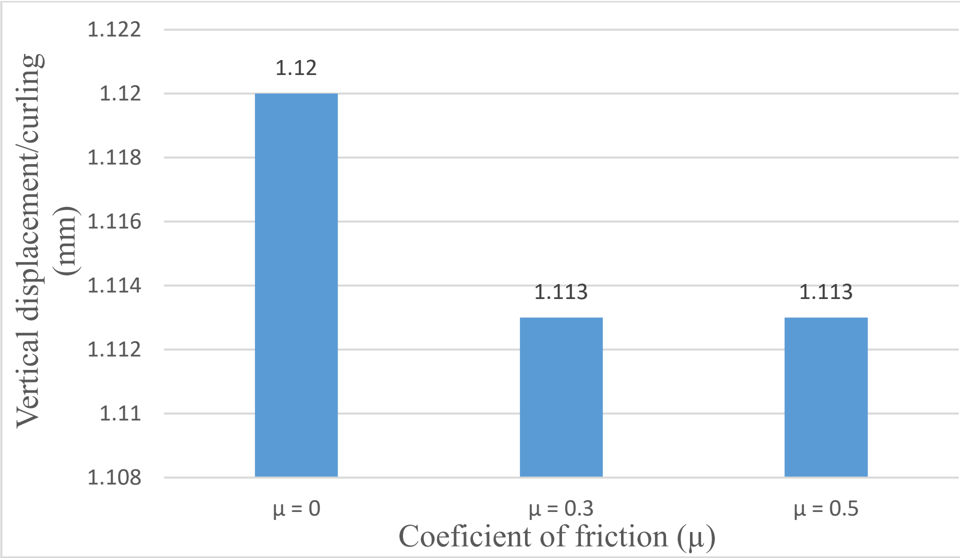

(a).

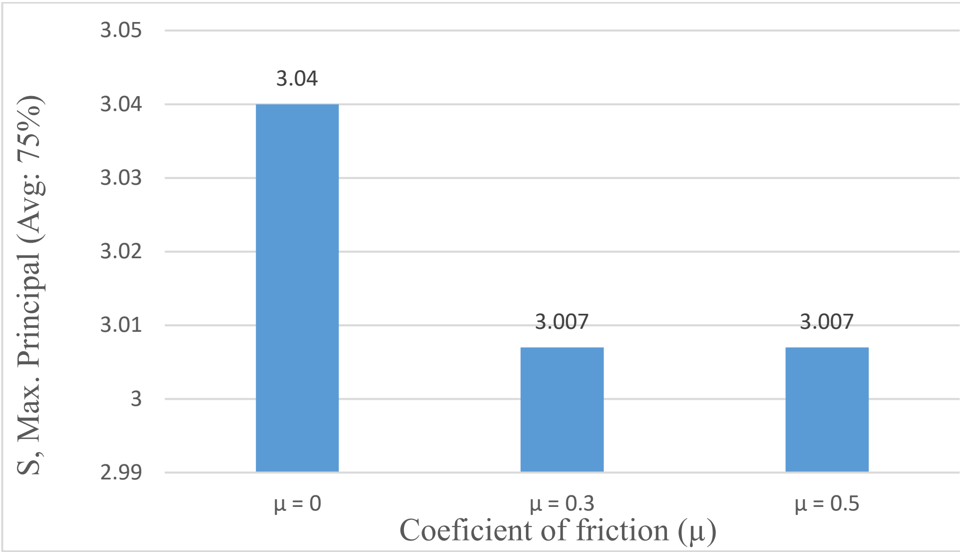

(b).

Figure 4. 17 Displacement (a) & stress (b) charts for different coefficients of friction.

4.3.9 Boundary conditions

For shrinkage strains to cause stresses in a structure, there must be some kind of restraints from the geometrical shape or supports. Shrinkage strains of concrete slabs-on-ground are restrained internally by reinforcement bars and gradient shrinkage strain as well as externally by supporting soils or walls. These strains may induce tensile stresses and tensile damage in concrete members and lead to cracks due to excessive shrinkage strain. There is maximum deflection and minimum stress for all ends free slabs and maximum stress with a minimum deflection for all ends restraint (Figure 4.18).

(a). 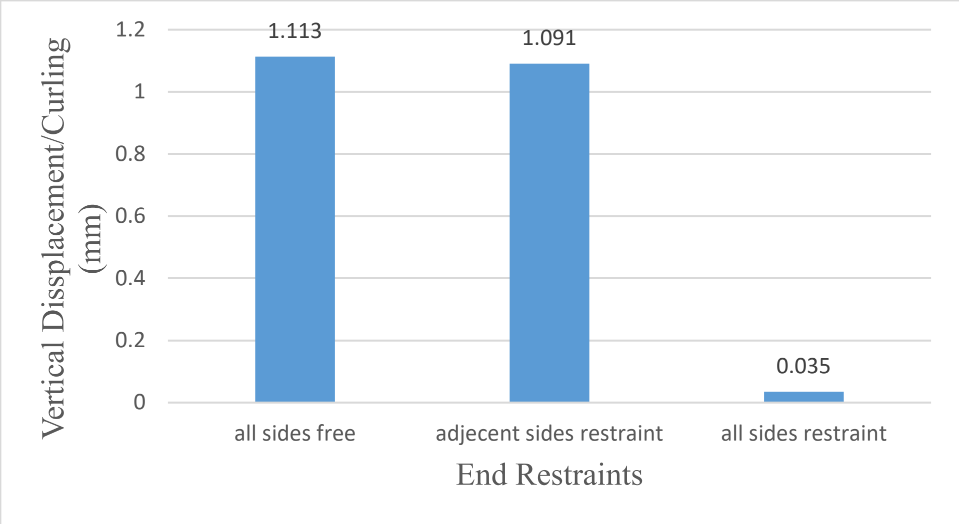

(b). 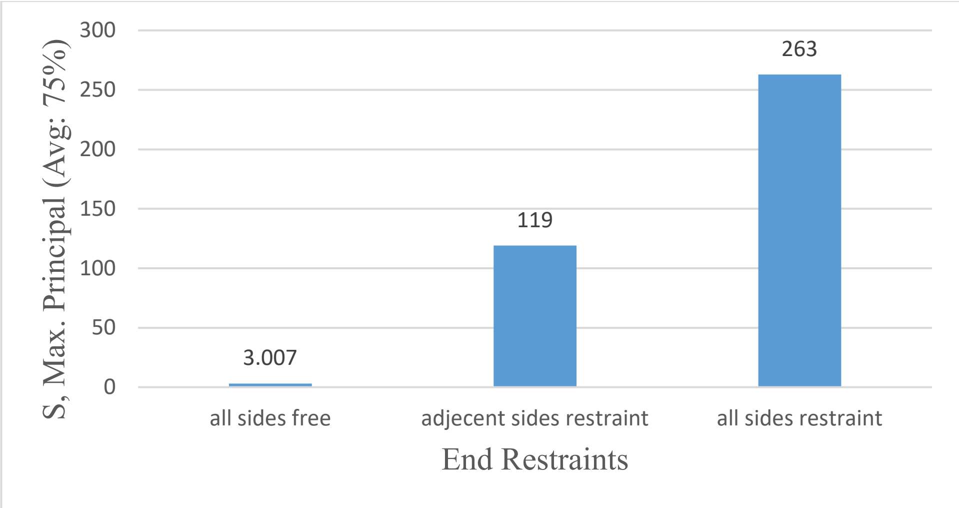

Figure 4. 18 Displacement (a) and stress (b) charts for different boundary conditions.

4.3.10 Positive temperature gradient, drying from the sun

The most common positive temperature gradient with its downward edge curling is that caused by heat from the sun on the upper slab surface (Figure 4.19). As seen from Figure 4.20 the slab linearly deflects downward at the corner and upward at the center.

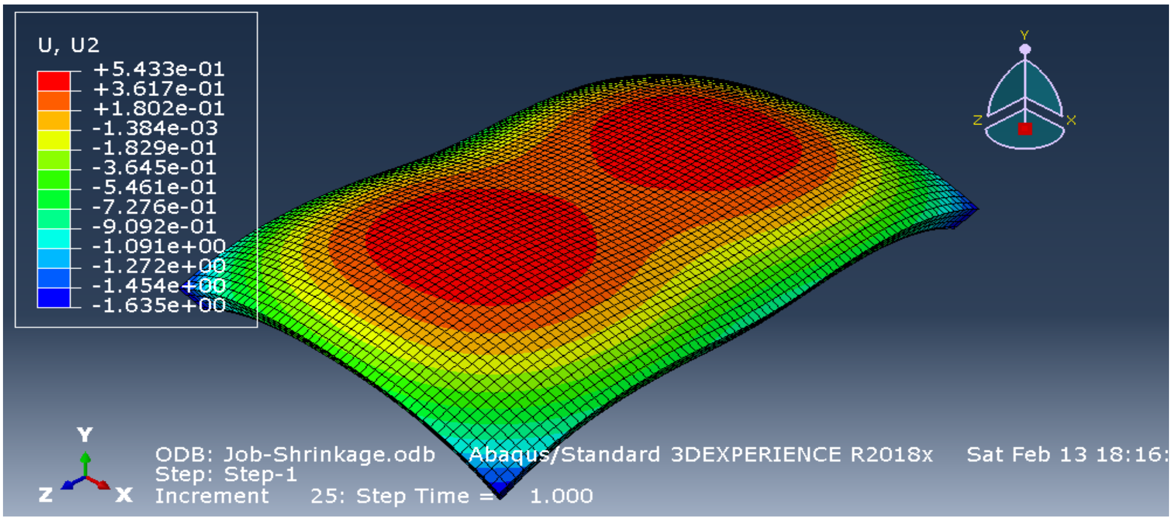

Figure 4. 19 Curling of slab-on-ground exposed to sun, positive temperature gradient.

(a).

(b).

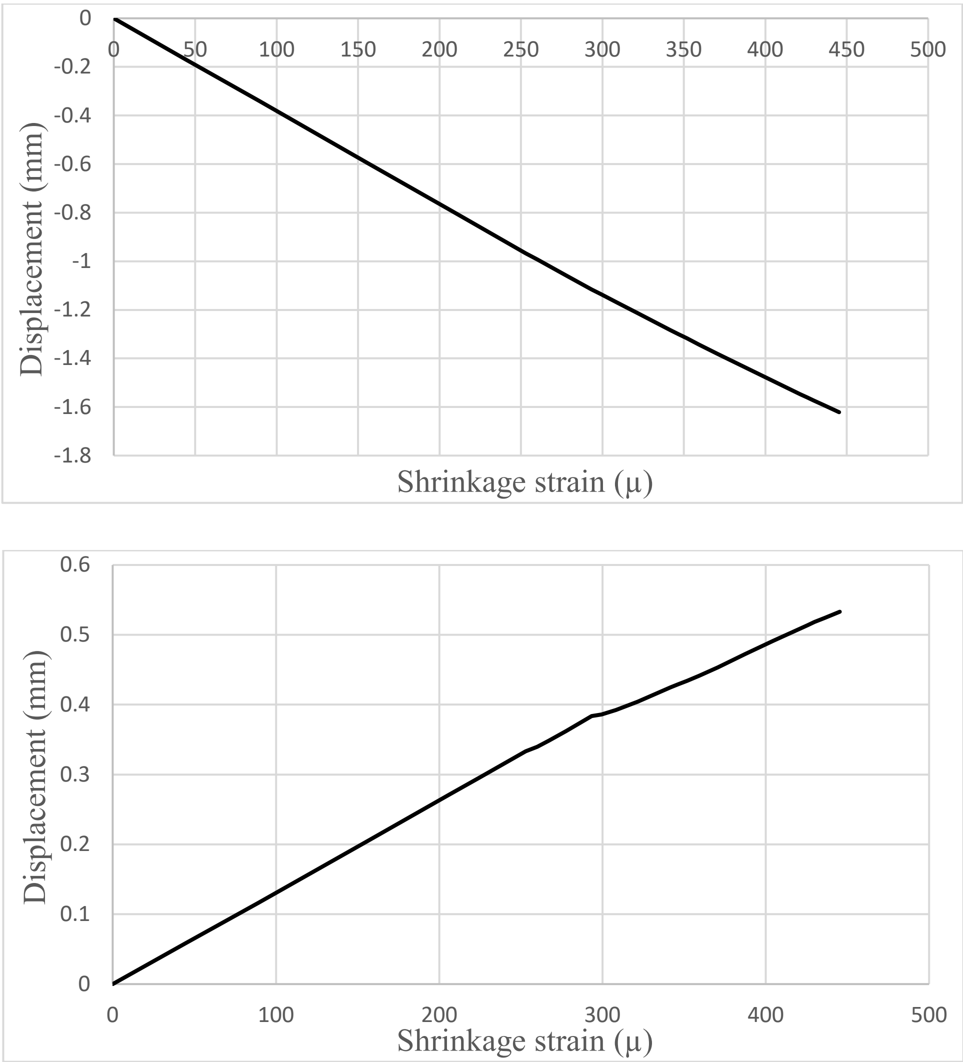

Figure 4. 20 Curling of slab at corner (a) & center (b) due to positive temperature gradient.

4.4 Discussion

The slab length and thickness were varied and the deflection and stress were compared. As shown in Figure 4.9 the length of the slab does not have a considerable effect on the maximum principal stress which is similar to (Prakash, 2018) statement. As the slab thickness increased vertical deflection and tensile damage in the slab also increased as shown in Figure 4.10. The reason is due to the effect of thickness on shrinkage load, as larger shrinkage strain will be developed with the increase in thickness. Increasing the thickness of the slab results in a larger shrinkage load as (Prakash, 2018) stated. For thin slabs almost no damage and high damage observed for thick slabs-on-ground, keeping other parameters constant.

The concrete strength class affects the functionality of the slabs-on-ground in curling and principal stress due to differential shrinkage strain. Lower strength concrete classes have less vertical displacement and principal stress. And higher strength class of concrete has high vertical deflection/curling and high principal stress (Ytterberg, 1992) also stated.

Cracks can be avoided by varying the reinforcement position in the slab and for more practical use, reinforcements are positioned in the bottom of the slab with a concrete cover of 20mm. From Figure 4.12 it can be inferred that by applying reinforcement in the half depth of the slab, both damage (i.e crack) and vertical displacement can be decreased.

At the interface between the slab and ground, there will be friction, which should result in deflection and stress. Nonlinear model results presented in Figure 4.17 indicate that when the slab rests on the frictionless ground, maximum vertical deflection and maximum principal stress are significantly affected. Thereby, varying the frictional coefficient between concrete and ground at the interface vertical displacement and stress will vary.

As relative humidity increases, moisture on the concrete surface increases and drying will be decreased. Higher relative humidity in the ambient air at the upper surface will reduce the severity of curling even though the concrete may be a high shrinkage material. Shrinkage strain will be reduced so that vertical displacement also decreased (Figure 4.13a). Also, maximum principal stress decreases as relative humidity increases (Figure 4.13b).

Applied external loads enhance the situation by decreasing the vertical deflection, while the tensile damage decreases for increasing load steps, as a result, compression damage increases at the location of the load, (Øverli, 2014) also prove this in his experimental work.

Shrinkage strains of concrete slabs-on-ground cause high stress and crack on the slab surface when restrained externally. There is maximum deflection and minimum stress for all ends free slabs and maximum stress with a minimum deflection for all ends restraint (Figure 4.18) as (Fabian Narin and Olle Wiklund, 2012) proved. The result presented in Figure 4.15, shows that displacement decreases as sub-grade stiffness (modulus of subgrade) increases.

Slabs on the ground may curl either upward or downward, caused by negative moisture gradient and positive temperature gradient respectively. The most common positive temperature gradient with its downward edge curling is that caused by heat from the sun on the upper slab surface (Figure 4.19). As seen from Figure 4.20 the slab linearly deflects downward at the corner and upward at the center as (Ytterberg, 1992) stated.

CHAPTER FIVE

CONCLUSION AND RECOMMENDATION

5.1 Conclusion

Vertical deflection and stress of slabs-on-ground are undesired events that reduce the performance and durability of the slabs. In this thesis, non-linear finite element analyses were performed to study the principal stress, tensile damage, and vertical deflections, obtained through finite element modeling (FEM) using the general-purpose software ABAQUS/CAE 2018 to investigate the influence from the shrinkage gradient in reinforced concrete slabs on the ground.

One of the objectives of the thesis was to develop an accurate non-linear finite element model to predict the maximum principal stress, tensile damage, and deflection behavior of concrete slabs-on-ground and to study the effects of gradient shrinkage. Maximum principal stress and deflection, which are common calamities in different types of slabs-on-ground associated with gradient shrinkage have been studied. A further objective was to perform parametric studies were performed to analyze the response of varying length, thickness, and concrete strength class, and relative humidity, reinforcement position, drying condition, external load cases, and friction between slab and sub-base on principal stress, tensile damage, and deflection.

The general purpose software ABAQUS/CAE 2018 was used here for the non-linear finite element analyses since it is specially developed for nonlinear finite element analysis of any structures. The finite element analyses confirm the importance of slab thickness concerning gradient shrinkage so that a thicker slab will result in larger deflection and stress. For different concrete strength classes and varying reinforcement positions for certain slab thickness, the maximum stress and vertical deflection were studied. As concrete strength increased, maximum stress and vertical deflection also increased. It was estimated that upward curling occurred as a result of more contraction of the top of the slab than that of the bottom owing to the moisture evaporation. Besides, a larger deformation occurred near the slab corner than at other positions because that is what happens when two adjacent, perpendicular edges in a flat plane both roll upward. The parametric studies also showed that the friction parameter at the interface influences the stress and deflection of concrete slab associated with shrinkage gradients.

This study was conducted to analyze the shrinkage behavior of slabs on the ground concerning different parameters. It was found that all parameters significantly affect the vertical deflection/curling and principal stress of slabs on the ground due to differential shrinkage strain. Therefore, it was possible to conclude that vertical deflection/curling, principal stress, and damage (or cracking) are inevitable in slabs on the ground due to differential shrinkage strain.

5.2 Recommendations for Future Research

During this thesis work, several assumptions and limitations were considered for studying the gradient shrinkage strain effect. Based on knowledge gained throughout this thesis, some interesting insights for further studies have emerged. It will be interesting to further develop a model to study the effects of early-age temperature and shrinkage effects of slab-on-ground. The time-dependent effect of creep and stress relaxation on shrinking slabs-on-ground might provide more information about the deformation and stress behavior. Comparison of the model with experimental results might help to further evaluate the accuracy of the model and its development.

REFERENCES

Abaqus 6.13 Manual. (2017). *Abaqus Analysis User's Guide.* Retrieved from Abaqus Version 6.13 Documentation Collection.

ACI 209.2R-08. (2008). *Guide for Modeling and Calculating Shrinkage and Creep in Hardened Concrete.* Reported by ACI Committee 209.

ACI 209R-92. (1992). *Prediction of Creep, Shrinkage and Temprature Effects in Concrete Structures.* Reported by ACI Committee 209.

ACI 360R-10. (2010). *Guide to Design of Slabs-on-Ground.* Reported by ACI Committee 360.

Ahmed, A. (2014). Modeling of a Reinforced Concrete Beam Subjected to Impact Vibration Using ABAQUS. *International Journal of Civil and Structural Engineering, 4*(3), 227-236. doi:10.6088/ijcser.201304010023

Al-Azzawi, A. A. (2018). Hollow Core Slabs on Winkler Foundation. *Journal of Engineering and Technological Sciences, 50*(6), 778-796. doi:10.5614/j.eng.technol.sci.2018.50.6.3

Ali N. Attiyah, Hans Gesund, and Mohammed H. Rasool. (2013). Finite Element Modelling of Concrete Shrinkage Cracking in Walls. *Kufa Journal of Engineering (K.J.E), 5*(1), 127-140.

Amir M. Alani and Morteza Aboutalebi. (2012). Analysis of the Subgrade Stiffness Effect on the Behaviour of Ground-Supported Concrete Slabs. *Structural Concrete, 13*(2), 102 - 108. doi:DOI: 10.1002/suco.201100043

B. Alfarah, F. López-Almansa, and S. Oller. (2016). New Methodology for Calculating Damage Variables Evolution in Plastic Damage Model for RC Structures. *Engineering Structures*, 70-86. doi:http://dx.doi.org/10.1016/j.engstruct.2016.11.022

B. Belletti, R. Cerioni, A. Meda, and G. A. Plizzari. (2004). Experimental and Numerical Analyses of FRC Slabs on Grade. *Department of Civil Engineering, Italy*.

Desai, P. (2011). Drying Shrinkage Behaviour of Foam – Cement Panel. *Navrachana University, Bhayli, Vadodara*.

ES EN. (1992:2015). *Design of Concrete Structures-Part 1-1, General Rules and Rules for Buildings.* Addis Ababa, Ethiopia: Ethiopian Building Code Standard.

Fabian Narin and Olle Wiklund. (2012). Design of Slabs-on-Ground Regarding Shrinkage Cracking. *MSc. Thesis, Chalmers University of Technology*, P199.

Fib Model Code. (2013). *fib Model Code for Concrete Structures.* International Federation for Structural Concrete.

Freidriks, A. (2015). Prediction Models of Shrinkage and Creep in Industrial Floors and Overlays. *MSc. Thesis, Royal Institute of Technology*, P97.

Gardner, N. J. and Lockman, M. J. (2000). Design Provisions for Drying Shrinkage and Creep of Normal Strength Concrete. *ACI Materials Journal*, 159-167.

Gilbert, R. I. (2017). Cracking Caused by Early-Age Deformation of Concrete Prediction and Control. *Electronic Journal of Structural Engineering*, 13-22. doi:10.1016/j.proeng.2017.02.012

Giuseppe Tiberti, Antonio Mudadu, Bryan Barragan and Giovanni Plizzari. (2018). Shrinkage Cracking of Concrete Slabs-On-Grade: A Numerical Parametric Study. *Fibers, 6*(64), P18. doi:10.3390/fib6030064

Gunalan, K. N. (1986). Analysis of Industrial Floor Slabs-on-Ground for Design Purposes. *PhD. Thesis, Faculty of Texas Tech University*, P273.

Jafarifar, N. (2012). Shrinkage Behaviour of Steel Fiber Reinforced Concrete Pavements. *PhD Thesis, The University of Sheffield*. Retrieved from Abaqus Version 6.13 Documentation Collection.

Jin-Hoon Jeong, Joo-Young Park, Jin-Sun Lim and Sung-Hee Kim. (2014). Testing and Modelling of Friction Characteristics Between Concrete Slab and Subbase Layers. *Road Materials and Pavement Design, 15*(1), 114-130. doi:http://dx.doi.org/10.1080/14680629.2013.863161

Karschner, K. A. (2012). Effects of Creep and Shrinkage on Time-Dependent Strain and Curvature of RC Members. *MSc. Thesis, The Pennsylvania State University*, P114.

Konstantin Kovler and Nicolas Roussel. (2011). Properties of Fresh and Hardened Concrete. *Cement and Concrete Research*, 775–792.

Labib, W. A. (2008). An Experimental Study and Finite Element Analysis of Punching Shear Failure in Steel Fiber-Reinforced Concrete Ground-Suspended Floor Slabs. *PhD. Thesis, Liverpool John Moores University*, P299.

Mala Babagana and Ani Abdulfatah. (2017). The Quantities of Materials in One Cubic Meter of Concrete Using Different Mix Ratios. *University of Maiduguri*, P28.

Marie Kozielova, Zuzana Marcalikova, Pavlina Mateckova, Oldrich Sucharda. (2020). Numerical Analysis of Reinforced Concrete Slab with Sub Soil. *Civil and Environmental Engineering, 0*(0). doi:10.2478/cee-2020-0011

Matin, D. J. (2015, March). Temprature and Shrinkage Cracking in Reinforced Concrete Walls. *PhD. Thesis, Toronto, Ontario, Canada*, P218.

N. Mailvaganam, J. Springfield, W. Repette and D. Taylor. (2000, December). Curling of Concrete Slabs on Grade. *Institute for Research in Construction, IRC*. Retrieved from http://www.nrc.ca/irc

Nejadi, S. (2005, March). Time-Dependent Cracking and Crack Control in Reinforced Concrete Structures. *PhD. Thesis, Sydney, Australia*, P408.

Øverli, J. (2014). Experimental and Numerical Investigation of Slabs on Ground Subjected to Concentrated Loads. *Central European Journal of Engineering*. doi:10.2478/s13531-013-0159-9

P J Robins, J W Bishop and S A Austin. (2003). Early-Age Finite Element Modelling of Industrial Ground Floors. *Materials*, 295-308.

Prakash, S. (2018). Nonlinear Finite Element Analysis of Shrinking Reinforced Concrete Slabs-on-Ground. *MSc. Thesis, Royal Institute of Technology*, P124.

Rao, S. S. (2018). *The Finite Element Method in Engineering, Sixth Edition.* University of Miami, Coral Gables, FL, United States.

Rebello, K. J. (1990). Analysis for Creep, Shrinkage and Temperature Effects on Expansion Joint Movements in Composite Prestressed Concrete Bridges. *PhD. Thesis, Louisiana State University*, P320. Retrieved from https://digitalcommons.lsu.edu/gradschool_disstheses/5019

Shideh Shadravan, Chris Ramseyer and Thomas H.-K. Kang. (2015). A Long Term Restrained Shrinkage Study of Concrete Slabs on Ground. *Engineering Structures*, 258-265. doi:http://dx.doi.org/10.1016/j.engstruct.2015.08.018

Telford, T. (1993). *CEB-FIP Model Code.* Euro-International Committee for Concrete.

Wahalathantri, B.L, Thambiratnam, D.P, Chan, T.H.T, and Fawzia,S. (2011). A Material Model for Flexural Crack Simulation in RC Elements Using ABAQUS. *Queensland University of Technology, Brisbane, Australia*, 260-264.

Ytterberg, R. F. (1992). Control of Shrinkage and Curling in Slabs on Grade.

Zdeněk P. Bažant and Sandeep Baweja. (2000). Creep and Shrinkage Prediction Model for Analysis and Design of Concrete Structures. *Materials and Structures*.

APPENDICES

Appendix A: Factors & Variables in Shrinkage Prediction Models

Table A. 1 Factors and variables affecting considered in ACI 209R-92.

Factors			Variables Considered	Standard Conditions
Concrete (Shrinkage)	Concrete composition	Cement paste content	Type of cement	Type I & III
		Water-cement ratio	Slump	70 mm
		Mixture proportions	Air content	$\leq$ 6%
		Aggregate characteristics	Fine aggregate percentage	50%
		Degree of compaction	Cement content	279 to 446 kg/m^3
	Initial curing	Length of initial curing	Moist cured	7 days
			Steam cured	1 to 3 days
		Curing temperature	Moist cured	23.2 $\pm$ 2 ^{O}C
			Steam cured	$\leq$ 100 ^{O}C
		Curing humidity	Relative humidity	$\geq$ 95 %
Member geometry and environment (Shrinkage)	Environment	Concrete temperature	Concrete temperature	23.2 $\pm$ 2 ^{O}C
		Concrete water content	Ambient relative humidity	40 %
	Geometry	Size and shape	Volume-surface ratio or Minimum thickness	V/S = 38 mm 150 mm

Table A. 2 Shrinkage correction factors for initial moist curing, ACI 209R-92 Model.

Moist curing duration, t_c (days)	Shrinkage correction factor, $\Upsilon_{sh,tc}$
1	1.2
3	1.1
7	1.0
14	0.93
28	0.86
90	0.75

Table A. 3 Shrinkage correction factors for the average thickness of members, ACI 209R-92.

The average thickness of member, d (mm)	Volume surface ratio, V/S (mm)	The shrinkage correction factor, $\Upsilon_{sh,d}$
51	12.5	1.35
76	19	1.25
102	25	1.17
127	31	1.08
152	37.5	1.00

Table A. 4 Nominal drying shrinkage values $\varepsilon_{cd.o}$, (in ‰) for concrete of cement class N.

$f_{ck}/f_{ck,cube}$ (MPa)	Relative humidity (%)					
	20	40	60	80	90	100
20/25	0.62	0.58	0.49	0.30	0.17	0.00
40/50	0.48	0.46	0.38	0.24	0.13	0.00
60/75	0.38	0.36	0.30	0.19	0.10	0.00
80/95	0.30	0.28	0.24	0.15	0.08	0.00
90/105	0.27	0.25	0.21	0.13	0.07	0.00

Table A. 5 values for k_h

h_o	k_h
100	1.0
200	0.85
300	0.75
$\geq$ 500	0.70

Table A. 6 Humidity dependence factor k_h, B3-model.

Relative humidity, h (decimal)	k_h
$h \leq 0.98$	$1 - h^3$
h = 1.00 (swelling in water)	- 0.2
0.98 < h < 1.00	Linear interpolation: 12.75 – 12.95h

Table A. 7 α_1 as a function of cement type, B3 model.

Type of cement	α_1
Type I	1.00
Type II	0.85
Type III	1.10

Table A. 8 α_2 as a function of curing condition, B3 model.

Curing method	α_2
Steam cured	0.75
Cured in water or at 100% relative humidity	1.00
Sealed during curing or normal curing in the air with initial protection against drying	1.20

Table A. 9 k_s as a function of cross-section shape, B3 model.

Cross-section shape	k_s
Infinite slab	1.00
Infinite cylinder	1.15

Infinite square prism	1.25
Sphere	1.30
Cube	1.55

Table A. 10 Values for coefficient β_{sc} , CEB MC90 model.

Type of Cement according to EC2	β_{sc}
SL (slowly-hardening cements)	4
N and R (normal or rapid hardening cement)	5
RS (rapid hardening high-strength cement)	8

Table A. 11 Values for coefficients α_{ds1} and α_{ds2} , CEB MC90-99 and fib model code 2010.

Type of Cement according to EC2	α_{ds1}	α_{ds2}	α_{as} α_{bs}
SL (slowly-hardening cements)	3	0.13	800
N and R (normal or rapid hardening cement)	4	0.12	700
RS (rapid hardening high-strength cements)	6	0.12	600

Table A. 12 Parameter k as a function of cement type, GL2000 model.

Cement type	*K*
Type I	1.0
Type II	0.75
Type III	1.15

Appendix B: Shrinkage Strain Prediction Models

Table B. 1 Bazant-Bawja, B3 model for typical C30/37 concrete.

Time (day)	$\sqrt{\frac{t-t_c}{\tau_{sh}}}$	$S(t-t_c)$	$\varepsilon_{sh}(t,t_c)$ (mm/mm)	$\varepsilon_{sh}(t,t_c)$ (μ strain)
7	0	0	0	0
14	0.064403	0.064314	-4.6E-05	-45.6984
28	0.111549	0.111089	-7.9E-05	-78.9343
60	0.177212	0.17538	-0.00012	-124.617
90	0.221766	0.218201	-0.00016	-155.043
180	0.320169	0.30966	-0.00022	-220.029
365	0.460572	0.43055	-0.00031	-305.928
400	0.482561	0.448292	-0.00032	-318.535
450	0.51234	0.471766	-0.00034	-335.214
500	0.54048	0.493351	-0.00035	-350.552
700	0.6408	0.565444	-0.0004	-401.778
1000	0.767063	0.645218	-0.00046	-458.461
1300	0.875297	0.704055	-0.0005	-500.268
1600	0.971548	0.749384	-0.00053	-532.476
2000	1.0867	0.795671	-0.00057	-565.365
2500	1.215395	0.83829	-0.0006	-595.649
3000	1.33171	0.869667	-0.00062	-617.943
3500	1.438651	0.893426	-0.00063	-634.826
4000	1.538175	0.911813	-0.00065	-647.891
4500	1.63164	0.926295	-0.00066	-658.181
5000	1.720034	0.937867	-0.00067	-666.403
5500	1.804101	0.947229	-0.00067	-673.056
6000	1.884423	0.954884	-0.00068	-678.495
7000	2.035579	0.966457	-0.00069	-686.718
8000	2.176261	0.974579	-0.00069	-692.489
9000	2.308386	0.980424	-0.0007	-696.642
10000	2.433347	0.98472	-0.0007	-699.695

12000	2.665754	0.990373	-0.0007	-703.712
15000	2.980578	0.994859	-0.00071	-706.899
17000	3.173154	0.9965	-0.00071	-708.065
20000	3.441875	0.997954	-0.00071	-709.098

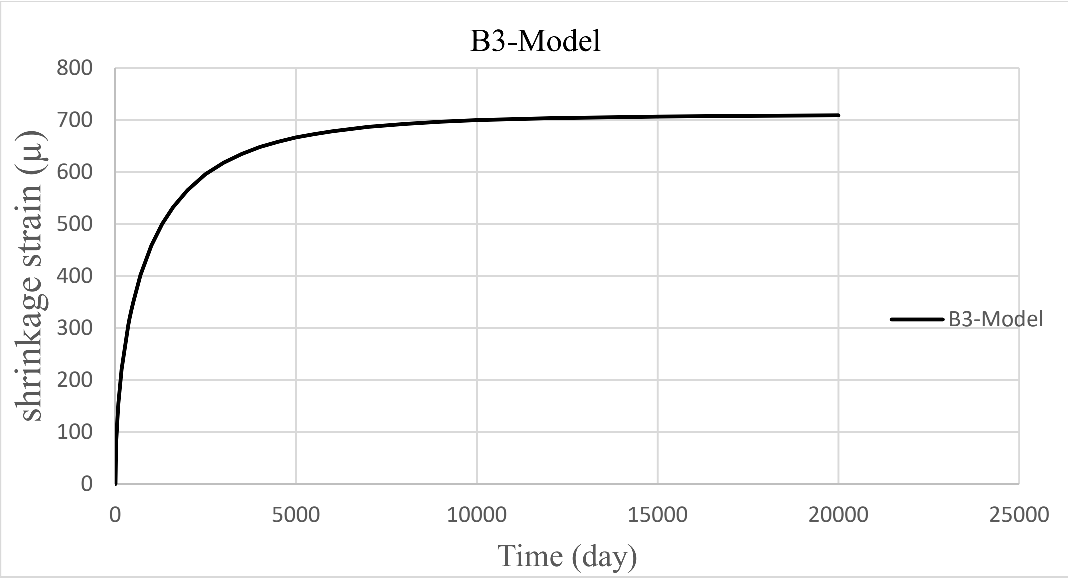

Figure B. 1 Bazant-Bawja, B3 model curve.

Table B. 2 GL2000 model for typical C30/37 concrete.

Tme (day)	$\beta(t - t_c)$	$\mathcal{E}_{sh}(t, t_c)$ (mm/mm)	$\mathcal{E}_{sh}(t, t_c)$ (μ strain)
7	0	0	0
14	0.063518	4.93E-05	49.25941
28	0.109576	8.5E-05	84.97764
60	0.172507	0.000134	133.7815
90	0.214082	0.000166	166.0236
180	0.30167	0.000234	233.9494
365	0.414271	0.000321	321.2731
400	0.430453	0.000334	333.8227
450	0.451723	0.00035	350.3175
500	0.471139	0.000365	365.3752
700	0.535019	0.000415	414.915

1000	0.604102	0.000468	468.49
1300	0.65422	0.000507	507.3572
1600	0.692586	0.000537	537.1102
2000	0.731853	0.000568	567.5626
2500	0.768517	0.000596	595.9961
3000	0.796226	0.000617	617.4848
3500	0.817942	0.000634	634.3258
4000	0.835437	0.000648	647.8935
4500	0.849842	0.000659	659.0647
5000	0.861914	0.000668	668.4267
5500	0.87218	0.000676	676.3883
6000	0.881019	0.000683	683.2432
7000	0.895465	0.000694	694.4461
8000	0.906775	0.000703	703.217
9000	0.915872	0.00071	710.2718
10000	0.923348	0.000716	716.0701
12000	0.934913	0.000725	725.0383
15000	0.94692	0.000734	734.35
17000	0.952731	0.000739	738.8571
20000	0.959399	0.000744	744.0275

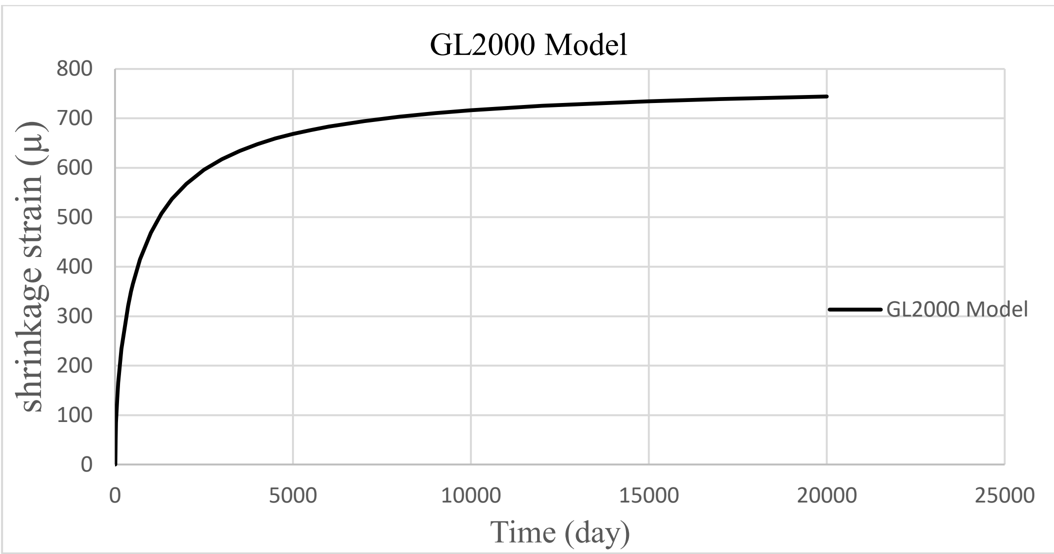

Figure B. 2 GL2000 model curve.

Table B. 3 CEB-FIP 90-99 model for typical C30/37 concrete.

Time	Drying shrinkage			Autogenous shrinkage			Total shrinkage
Day	$\beta_{ds}(t,t_c)$	$\mathcal{E}_{cds}(t,t_c)$ (mm/mm)	$\mathcal{E}_{cds}(t,t_c)$ (μ strain)	$\beta_{as}(t,t_c)$	$\mathcal{E}_{cas}(t,t_c)$ (mm/mm)	$\mathcal{E}_{cas}(t,t_c)$ (μ strain)	$\mathcal{E}_{sh}(t,t_c)$ (μ strain)
7	0	0	0	0.41089	-3E-05	26.9291	26.9291
14	0.07053	-4E-05	42.807	0.52684	-3E-05	34.5282	77.3353
28	0.12157	-7E-05	73.7778	0.65295	-4E-05	42.7932	116.571
60	0.19099	-0.0001	115.909	0.78758	-5E-05	51.6163	167.526
90	0.23657	-0.0001	143.576	0.85004	-6E-05	55.7096	199.285
180	0.33163	-0.0002	201.267	0.93166	-6E-05	61.059	262.326
365	0.45127	-0.0003	273.871	0.97809	-6E-05	64.1021	337.973
400	0.46817	-0.0003	284.131	0.98168	-6E-05	64.3374	348.469
450	0.49027	-0.0003	297.545	0.98563	-6E-05	64.596	362.141
500	0.51033	-0.0003	309.714	0.98858	-6E-05	64.7892	374.504
700	0.57542	-0.0003	349.217	0.99497	-7E-05	65.2079	414.425
1000	0.64417	-0.0004	390.946	0.99821	-7E-05	65.4204	456.366
1300	0.69292	-0.0004	420.527	0.99926	-7E-05	65.4894	486.017
1600	0.72955	-0.0004	442.759	0.99966	-7E-05	65.5158	508.275
2000	0.76641	-0.0005	465.131	0.99987	-7E-05	65.5292	530.66
2500	0.80024	-0.0005	485.66	0.99995	-7E-05	65.5348	551.195
3000	0.82542	-0.0005	500.94	0.99998	-7E-05	65.5367	566.477
3500	0.84491	-0.0005	512.773	0.99999	-7E-05	65.5373	578.31
4000	0.86047	-0.0005	522.213	1	-7E-05	65.5376	587.751
4500	0.87317	-0.0005	529.924	1	-7E-05	65.5377	595.461
5000	0.88375	-0.0005	536.342	1	-7E-05	65.5378	601.88
5500	0.89269	-0.0005	541.769	1	-7E-05	65.5378	607.306
6000	0.90035	-0.0005	546.418	1	-7E-05	65.5378	611.956
7000	0.91279	-0.0006	553.97	1	-7E-05	65.5378	619.508
8000	0.92247	-0.0006	559.843	1	-7E-05	65.5378	625.38
9000	0.93021	-0.0006	564.54	1	-7E-05	65.5378	630.078
10000	0.93655	-0.0006	568.384	1	-7E-05	65.5378	633.922

12000	0.94629	-0.0006	574.299	1	-7E-05	65.5378	639.837
15000	0.95635	-0.0006	580.401	1	-7E-05	65.5378	645.939
17000	0.96119	-0.0006	583.34	1	-7E-05	65.5378	648.878
20000	0.96673	-0.0006	586.7	1	-7E-05	65.5378	652.238

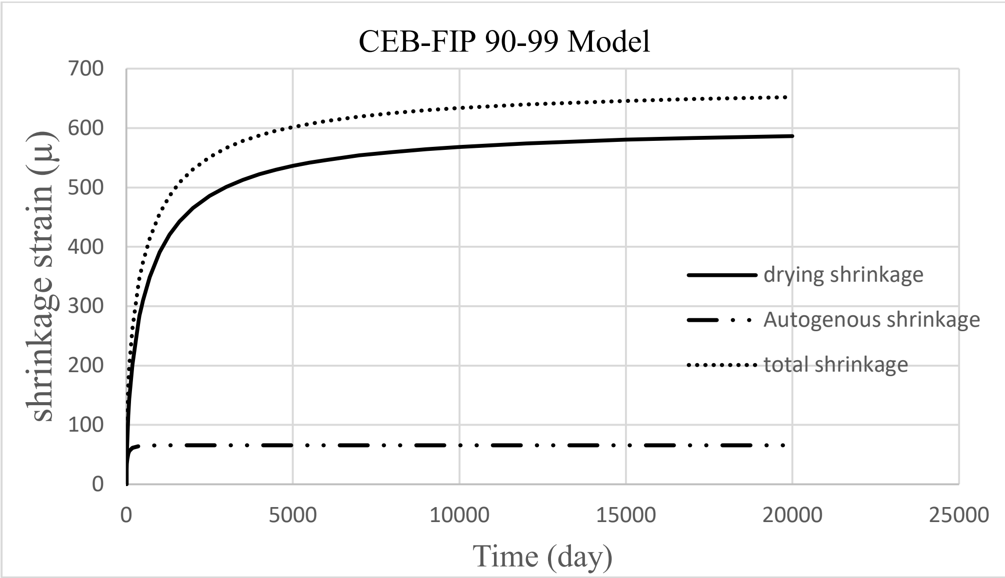

Figure B. 3 CEB-FIP 90-99 model curve.

Table B. 4 Model comparison for 360 days *(ACI 209.2R-08, 2008)*.

Time	Shrinkage strain (μ strain) for each models							
Day	B3	ACI 209R	GL2000	ES EN	fib 2010	CEB-FIP(dry)	CEB-FIP(auto)	CEB-FIP(total)
7	0	0	0	0	0	0	21.57277	21.57277
14	38.80243	109.0888	46.83473	59.57447	1.794113	31.90527	27.66038	59.56564
28	66.95131	280.7696	80.65373	137.7049	3.048299	54.98864	34.28141	89.27005
60	105.4448	336.5884	126.4838	227.957	4.646439	86.39041	41.34953	127.7399
90	130.9002	344.1344	156.4222	269.9187	5.609575	107.0111	44.62861	151.6397
180	184.5855	348.2727	218.3034	324.8826	7.368975	150.0096	48.91405	198.9237
365	253.5776	349.2352	294.802	359.799	9.110868	204.1232	51.35185	255.4751